

CONTENTS:

| | |
|--|---------|
| Abstract | page 1 |
| I. Introduction/Statement of the Problem | page 1 |
| II. Approach to the Problem | page 3 |
| III. Details of the Integration | page 4 |
| IV. Results | page 11 |
| V. Conclusion/Summary | page 25 |
| VI. Figures and Figure Captions | page 28 |
| VII. References | page 30 |
| VIII. Acknowledgments | page 32 |
| Appendix | page 32 |

A Simulation to Study Speed Distributions in a Solar Plasma

ABSTRACT

We (Peter Cheeseman of NASA Ames/Caelum Research) & Jose Luis Alvarelos of the SJSU Physics Department/SJSU Foundation.) have carried out a numerical simulation of a plasma with characteristics similar to those found in the core of the Sun. Particular emphasis is placed on the Coulomb interaction between the ions and electrons, which could result in a relative velocity distribution different from the Maxwell-Boltzmann (MB) distribution generally assumed for a plasma. The fact that the distribution may not exactly follow the MB distribution could have very important consequences for a variety of problems in solar physics, especially the neutrino problem. Very briefly, the neutrino problem is that the observed neutrino detections from the Sun are smaller than what the standard solar theory predicts [1]. In Section I we introduce the problem and in section II we discuss the approach to try to solve the problem: i.e., a molecular dynamics approach. In section III we provide details about the integration method, and any simplifications that can be applied to the problem. In section IV (the core of this report) we state our results, first for the specific case of 1000 particles and then for other cases with different number of particles. In section V we summarize our findings and state our conclusions. Sections VI VII and VIII provide the list of figures, reference material and acknowledgments respectively.

I. INTRODUCTION/STATEMENT OF THE PROBLEM

A plasma is a hot, ionized gas which is composed of (positive) ions and free electrons distributed over a region of space (Chen [2]; Spitzer [3]). Plasmas are electrically neutral (overall charge=0). Examples of plasmas are the ionosphere, which is an upper layer of the atmosphere, and the gas in the interior of the Sun. In the core of the Sun, temperatures are so high that atoms are completely stripped of their electrons, thereby constituting a plasma, composed of (positive) nuclei and free electrons.

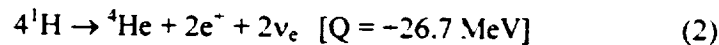
We wish to study the behavior of a plasma under the same conditions as in the Sun's core. The main interaction affecting the behavior of the ions and electrons in plasma is the

Coulomb Force. Much of the work done in Plasma Physics/Solar Physics assumes a MB speed distribution for the ions and electrons. The MB speed distribution is

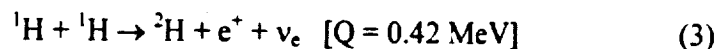
$$g(v) = 4n\pi(m/2\pi k_B T)^{3/2} v^2 \exp(-v^2/v_{th}^2) \quad (1)$$

where n is the number density, k_B is Boltzmann's constant, T the temperature and we define $v_{th}^2 \equiv 2k_B T/m$. The quantity $g(v)dv$ gives the number of particles per unit volume with a speed between v and $v + dv$. Analytical derivations of the MB distribution assume that all of the energy is kinetic energy, that is, the classical derivation neglects any inter-particle forces such as the Coulomb force. A measure of the deviation from "ideal gas" conditions is the parameter Γ which will be defined later; suffice it to say that for an ideal gas, $\Gamma = 0$, and for a real plasma $\Gamma > 0$. There will be deviations from MB due to the Coulomb interaction, the question is how much (Swihart [4]). For another view on the effects of a non-MB distribution on solar neutrino rates see Clayton (refs. [5] and [6]).

Energy production in the Sun is by thermonuclear reactions, primarily via the proton-proton (PP) chain. There are three possible PP chains (PPI, PPII and PPIII) and which dominates depends primarily on temperature (Clayton, 1983, [7]). In the overall view, the PP chain amounts to the combination of four protons to produce a ${}^4\text{He}$ nucleus, two positrons and two (electron) neutrinos (Bahcall 1989 [8]):

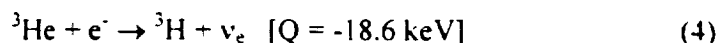


Of the 26.7 MeV released, only about 0.6 MeV is carried away by the neutrinos. The reaction is not as straightforward as implied by the above equation, which is a simplified view of the whole chain. The PP chain involves several "branches", such as the first branch of the PP chain:



For the rest of the branches see (Clayton, 1983 [7]) or (Bahcall, 1989, [8]).

The alternative reaction we are interested in is (Bahcall & Wolf, 1963 [9])



This is an electron capture by a ${}^3\text{He}$ nucleus to give a Tritium nucleus plus a neutrino. This reaction is not part of the standard solar model; note that it is endothermic and would release neutrinos of very low energy, lower than present "neutrino telescopes" would detect. If this reaction were to "go", the energy would have to be provided by the electrons, which would need an average energy of 18.6 keV. At the core of the Sun (1.56×10^7 K) the mean kinetic energy of electrons is 2 keV. *Assuming a MB distribution* the ratio of electrons with energy 18.6 keV to those with 2 keV is approximately 1.31×10^{-5} . In Ref. [9], Bahcall & Wolf imply that the reaction ${}^3\text{He}(e^-\nu_e){}^3\text{H}$ is only important in the case that the central density of a star $\rho_c > 2 \times 10^7 \text{ Kg/m}^3$, and so would proceed at a negligible rate in the Sun's core, where $\rho = 1.48 \times 10^5 \text{ Kg/m}^3$. However, they did not take into account the statistical mechanics of interacting particles. We suspected that the mean energy of electrons may be higher than 2 keV, which would make the electron capture reaction given above to be much more likely than the standard solar model predicts. A possible cause for deviations from MB distribution are the Coulomb interactions between electrons and ions. Another possible cause is electron degeneracy (see Swihart, 1972 [4]), but we concentrate on the effect of Coulomb interactions here. This is the purpose of the simulation.

II. APPROACH TO THE PROBLEM

We have developed a numerical model of a plasma, with characteristics typical for the interior of the Sun; i.e., the plasma will have the same temperature and density ($T = 1.56 \times 10^7$ K, $\rho = 1.48 \times 10^5 \text{ Kg/m}^3$, see Bahcall [8]), as the core of the Sun. We used a Molecular Dynamics (MD) simulation of electrons and ions (Haile [10]), using paired electron-ion "clusters" (as dipoles) to cut off field contributions below a given threshold. We use the Velocity-Verlet scheme to advance the system in time. It is reasonably fast and quite accurate. The simulation consists of a large number of ions and electrons in a given volume (determined by the density in the Sun's core) using periodic boundary conditions. We ignore quantum effects. We are investigating the following (among other things):

1. The possibility of a non-Maxwellian velocity distributions (ions and electrons) due to the long-range effects of the Coulomb force. This (possibly) non-Maxwellian distribution can affect the rate of certain nuclear reactions occurring in the Sun's core which are very important for the solar neutrino problem.
2. Check the relaxation times for ion-ion and ion-electrons interactions.
3. We will also check the (analytical) mean-free-path formula for ions and electrons.

III. DETAILS OF THE INTEGRATION

(a) Units

We choose to use atomic units or au (see McQuarrie [11]) as the most natural set of units for the problem at hand. The unit of length is the Bohr radius, the unit of mass is the electron's mass, etc. See the following table:

Table I: Atomic Units

| Quantity | Atomic Unit | MKS Equivalent |
|---------------|-------------------------------|-----------------------------|
| <i>Mass</i> | $m=1$ (electron mass) | 9.1091×10^{-31} Kg |
| <i>Charge</i> | $ e =1$ (electron charge) | 1.6021×10^{-19} C |
| <i>Length</i> | $a_o = 1$ (bohr) | 5.2918×10^{-11} m |
| <i>Time</i> | Electron period in Bohr orbit | 2.4189×10^{-17} s |
| <i>Energy</i> | 1 hartree | 4.35944×10^{-18} J |

Only temperature is the same as in the MKS set, i.e.. it is measured in degrees Kelvin.

(b) Initial Conditions

Since one of the things we want to check are the relaxation times, we choose initial conditions which are as far removed from equilibrium as possible, and then we see how long it takes for the system to relax. The initial positions are arranged in an FCC (Face-Centered-Cubic) pattern, as in a NaCl crystal, with electrons and protons at alternate positions. The total number of particles N_p is constrained by the fact that we want the overall charge to be zero. If we assume we have only electrons and protons, as in our case, this means that the total number

of particles has to be an even number. Furthermore, since we are using an FCC pattern, the cubic root of the total number of particles has to be an integer: this is the number of particles on a side of the computational box. Therefore, N_p is constrained by the following conditions:

- N_p is even
- $(N_p)^{1/3}$ is an integer

Using these criteria we find that $N_p = 8i^3$, with $i=1,2,3, 4, 5, \text{ etc.}$, so $N_p = 8, 64, 216, 512, 1000, 1728, \text{ etc.}$

The initial spacing d between each electron and proton in the lattice is determined from the Wigner-Seitz radius a , or

$$a = \left(\frac{3}{4\pi n_i} \right)^{1/3} \quad (5)$$

where n_i is the ion number density (equal to the electron number density). If we assume only Hydrogen is present, we obtain $a = 0.26$. As previously mentioned, a measure of the Coulomb coupling strength is Γ , which is defined as the ratio of the average potential energy to the average kinetic energy, or for equilibrium conditions

$$\Gamma = \frac{2}{3k_B T a} \quad (6)$$

Using the previously obtained value of a , we find $\Gamma = 0.05$ (in au $k_B = 3.17606 \times 10^{-6}$ hartrees/K).

Since we are using a cubic computational box, it can be shown that the length of a side will be $L = dN_p^{1/3}$, so that the volume is $V = d^3 N_p$. The number density of ions n_i is

$$n_i = \frac{\text{number of protons}}{\text{Volume of comp. box}} = \frac{N_p/2}{d^3 N_p} = \frac{1}{2d^3} \quad (7)$$

Substituting this expression into Eq. (5) and solving for d we obtain

$$d = \left(\frac{2\pi}{3} \right)^{1/3} a \quad (8)$$

Once we have decided the total number of particles and their initial positions we need to decide on their initial velocity. At first thought this seems simple: assign the initial velocities according to the average kinetic energy per particle at the center of the Sun (determined by the temperature). However, the average potential energy per ion-electron pair is lower at $t=0.0$ (for an FCC lattice) than for equilibrium conditions. This means that as the system evolves in time and approaches equilibrium, its potential energy will increase slightly. To conserve energy, the kinetic component has to decrease as the system evolves, which means the initial kinetic energy has to be slightly greater than the kinetic energy at equilibrium. We want the total energy per particle (after relaxation) to be equal to the mean kinetic energy per particle at the center of the Sun. The extra amount of kinetic energy is obtained by comparing the potential energy *per (proton-electron) pair* at $t = 0.0$, $u(0)$, and at equilibrium, $\langle u \rangle$. At $t = 0.0$ we have an FCC lattice, and the potential energy *per pair* is (in au's)

$$u(0) = -\left(\frac{\alpha}{a} \right) \left(\frac{3}{2\pi} \right)^{1/3} \cong -1.3659 / a \quad (9)$$

where $\alpha = 1.7476$ is the Madelung constant for an FCC lattice (see Ashcroft & Mermin [12]). At equilibrium, the average distance between an ion and an electron is the Wigner-Seitz radius, so

$$\langle u \rangle = -1 / a \quad (10)$$

The initial kinetic energy *per particle* $k(0)$ will be the kinetic energy at equilibrium $\langle k \rangle$ plus the difference between Eq. (9) & (10) divided by 2:

$$k(0) = \langle k \rangle + \frac{\langle u \rangle - u(0)}{2} \quad (11)$$

where $\langle k \rangle = 3k_B T / 2$. Since all particles have the same initial kinetic energy, the initial speed per particle will be $v(0) = \sqrt{2k(0)/m}$. Electrons will be faster than protons (by a factor of ~ 43) due to their lower mass. In effect, the initial speed distribution for electrons and protons is a delta function. The direction of the velocity vectors is chosen at random.

(c) Advancing the System in Time

Once the initial conditions are chosen (in the form of initial positions and velocities), the system is advanced in time via the Velocity-Verlet scheme (Allen & Tildesley 1992 [13] or Swope et al. [14]). Each particle $i=1,2,3,\dots,N_p$ is advanced in time as follows:

$$r_i(t+\Delta t) = r_i(t) + v_i(t) \bullet \Delta t + 0.5 \bullet [F_i(t) / m_i] \bullet \Delta t^2 \quad (12a)$$

$$v_i(t+\Delta t/2) = v_i(t) + 0.5 \bullet [F_i(t) / m_i] \bullet \Delta t \quad (12b)$$

$$v_i(t+\Delta t) = v_i(t+\Delta t/2) + 0.5 \bullet [F_i(t+\Delta t) / m_i] \bullet \Delta t \quad (12c)$$

where Δt is the (fixed) time-step size and (F_i/m_i) is the acceleration on particle i . The scheme is reasonably fast and very accurate: the local truncation error is $O(\Delta t^4)$. We use *periodic boundary conditions*: once a particle exits the computational box, it re-enters it on the opposite side.

(d) Forces

The computation of the forces on particle i is done as follows. A sphere centered on particle i with a “cut-off” radius R_c is chosen so that the forces on particle i of (most) particles outside of this sphere are ignored. Choosing the quantity R_c is a compromise between execution speed and accuracy, and must be found empirically; we chose to use $R_c = 0.67$. In addition, we keep charge neutrality for all the particles whose forces are acting on particle i (including particle i). If there is no charge neutrality within this sphere, we search outside the sphere for the nearest particles of the appropriate charge to keep the net charge zero. Thereafter, the force on particle i is

$$\mathbf{F}_i = \sum_{j'} \mathbf{F}_{ij} \quad (13)$$

where the sum goes from $j = 1, 2, 3, \dots, N_n$, where N_n is the number of “neighbors” of particle i (which varies as a function of time, but typically $\langle N_n \rangle \sim 40$ for $R_C = 0.67$) and \mathbf{F}_{ij} is the force on particle i due to particle j . The reason for the emphasis on charge neutrality is that we want to use paired electron-ion “clusters” (as dipoles) to cut off field contributions below a given threshold, as the field of a dipole falls off faster than that of a simple point charge. Finding which particles to use in the calculation of the forces on a particle (the “neighbors”) is computationally expensive, so we use the concept of *neighbor lists* to save time (see Haile, [10]). A list of the N_n neighbors of particle i is obtained and the same list is used over several consecutive time-steps to compute the forces. Typically we update the list every 15 time-steps

We use a modified form of the Coulomb interaction between two particles:

$$\mathbf{F}_{ij} = \frac{q_i q_j \mathbf{r}_{ij}}{(r_{ij}^2 + \epsilon^2)^{3/2}} \hat{\mathbf{r}}_{ij} \quad (14)$$

which, in the limit of small ϵ tends to the real Coulomb force. The main reason for this “softened” force is one of computational convenience, as it removes the possibility of the denominator in Eq. (14) from “blowing up” due to very close approaches. Another way to think of this softening is that each particle has a cloud of charge, 85% of which is contained within a radius of 3ϵ (see Sellwood [15]). Again, one must choose empirically a small enough value of ϵ so that Eq. (14) is a good approximation to the real Coulomb force, but not so small that close approaches between particles result in large errors (because of the finite size of the time-step Δt) due to extreme values of the denominator. We use $\epsilon = 2 \times 10^{-3}$.

The force between a “real” particle i (located inside the computational box, CB) and an “image” particle j' (a projection of a “real” particle j close to the opposite edge of the computational box from particle i) is handled by Haile’s “*Minimum Image Criterion*” (see [10]). This becomes important for particles close to the edge of the CB. This criterion identifies which of the multiple images of a real particle will be used in the computation of the

forces, and is applied separately to each cartesian component. For example, for the x component we have

$$\begin{aligned} x_j &\rightarrow x_j - L & (x_j < -L/2) \\ x_j &\rightarrow x_j + L & (x_j > L/2) \end{aligned}$$

and x_j is unchanged if $-L/2 \leq x_j \leq L/2$.

Finally, we mention that another computational “trick” to speed up the simulation is to use Newton’s Third Law whenever possible. If the force on particle j due to particle i F_{ji} is computed, then the force on particle i due to j F_{ij} does not need to be computed again as it is already known, i.e., $F_{ij} = -F_{ji}$ (along the same line!).

(d) Stochastic Heating

Stochastic Heating is a numerical artifact and is a result of all the errors in the computer simulation (due to truncation error, finite time-step, rounding off, finite computer precision, etc.). The result is that the mean kinetic energy per particle $\langle k \rangle$ increases as the simulation proceeds in time (see Hockney & Eastwood [16]). The average error in the kinetic energy $\langle h \rangle$ of, say, particle i , is a linear function of the number of time-steps n , and is given by

$$\langle h \rangle = \frac{[q_i \delta(\Delta t)]^2}{2m_i} n \quad (15)$$

where q_i is the particle’s charge, m_i is its mass, δ is the (modulus of the) error in the electric field (due to truncation, finite machine precision, etc.) computed at the location of particle i and Δt is the time-step used. It can be seen from Eq. (15) that the smaller the time-step, the smaller the effects of stochastic heating. Furthermore, the larger the mass, the less error in kinetic energy; hence, for a given time-step size, protons are much less affected (by a factor of $m_{\text{proton}}/m_{\text{electron}} \approx 1836$) than electrons by stochastic heating.

The result is that unless we provide corrections, the kinetic energy per particle (and hence the total system energy) will increase without bound. Therefore, we periodically check the error in the total energy and automatically provide corrections for stochastic heating by reducing the magnitude of the velocity vectors of all the particles. These corrections are different for protons than electrons.

(e) Table of characteristic lengths

Following is a table of the characteristic length scales involved in the problem. Also included is the Debye length, often-used in Plasma Physics work to indicate the “screening” effects of a collection of charges:

Table II: Characteristic Lengths for the problem

| Length | Value (au) |
|------------------------------------|------------------------|
| Wigner-Seitz radius, a , Eq. (5) | 0.26 |
| Lattice dist., d , Eq. (8) | 0.33 |
| Cut-off radius, R_c | $0.60 < R_c \leq 0.67$ |
| Softening radius, ϵ | 2.0×10^{-3} |
| Debye length, λ_D | 0.54 |

The significance of the Debye length is that for distances much greater than λ_D from a given charge, screening effectively cancels out the charge (see Chen, [2]). In addition, if the number of particles inside a “Debye” cube is much greater than unity, then the system is defined as a “collision-less” system (see [16]). In our case, the total number of particles in a Debye cube is $(\lambda_D/d)^3 \approx 4$. Therefore, collisions are important for our problem, as expected.

(f) Running the Programs

We implemented all of the previously mentioned ideas in the form of FORTRAN 77 codes. There are actually two versions of the program. The first version (main: PLSMMD.FOR) advances the system in time from $t = 0.0$ (FCC lattice, initial speed distribution is a delta function) to a sufficiently long enough time that the system is “well relaxed”. Along the way the program checks the speed distribution, conservation of energy and conservation of momentum. A time after which the system is “well relaxed” has been

found empirically and it is approximately 330.0 time units ($= 330.0 \times 2.4189 \times 10^{-17} \sim 8 \times 10^{-15}$ seconds). The second version (main: PLSMMD2.FOR) integrates the system in time from where the first program left off to an additional, arbitrary number of time steps. In this second version we check the speed distribution, energy conservation and close approaches. To speed up the simulation we skip momentum checking. The simulations are quite CPU intensive and a typical run could have lasted anywhere from a few days to a month depending on the total number of particles. The computer used was a 6-CPU, Ultra Enterprise 4000/5000 Sun Microsystems workstation with 1.2 GB of main memory running Solaris5.6. Both versions were compiled with Sun Microsystems' f77 compiler in double precision and optimized for speed (i.e., used the [-O4 -fast] compiler options). Each run took place on a single CPU, a 248 MHz UltraSPARC-II chip. See the Appendix for the programs and a discussion of the input parameters for these two programs.

IV. RESULTS

We have done several runs with different numbers of particles. In what follows we will discuss a typical case (with $N_p = 1000$ particles), state our results and then tabulate the same quantities using other values of N_p . Whenever possible we compare our answers with analytical expressions.

(a) Case $N_p = 1000$ particles (Relaxation Run):

We ran the first program, PLSMMD at the Unix prompt. This first program is run mainly to "relax" the system to equilibrium conditions, so we call this a "*relaxation run*". In **Figure 1** we see a plot of the initial positions and velocities in the computational box (CB). The length of a side the CB is $L = dN_p^{1/3}$, so for $N_p = 1000$ we have $L = 3.328$. The arrangement of electron-proton positions can easily be seen to be that of an FCC lattice: the circles with dots at the center are protons while the dots are electrons. The velocity vectors are also shown, although at this scale only the electron velocity vectors can be seen (the velocity vectors of the protons are approximately 43 times shorter). Note that the velocity vectors are randomly oriented, but the magnitude of all these vectors is the same (for a given species, obtained from Eq. (11)). For electrons this initial speed is $v_e(0) = 12.2322$ while for protons it is $v_p(0) = 0.2854$. In effect, the initial speed distribution is a delta function. It's easy to see that, apart from the orientation of the velocity vectors, there's nothing random about these

initial conditions. We now propagate this system forward in time using the Velocity-Verlet scheme. The time step size is $\Delta t = 1.1 \times 10^{-4}$, integrated for 3×10^6 time-steps. The softening radius is $\varepsilon = 2 \times 10^{-3}$ and the outer "cut-off" radius $R_c = 0.67$.

In **Fig. (2)** we see four panels with information related to the behavior of the energy for this first integration. In the first panel (**Fig. 2(a)**) we see the behavior as a function of time ($0.0 \leq t \leq 330.0$) of the total kinetic energy $K(t)$ (top line), the total system energy, both analytical and numerical, E and $E_n(t)$, (very close together appearing as one line, right below the kinetic energy) and the total potential energy $U(t)$ (bottom line, always negative). Note that most of the energy is kinetic, and it is this fact that makes plasma researchers ignore the potential energy of the system in some cases, assume ideal gas conditions, and hence use pure Maxwell-Boltzmann (MB) statistics. The two circles on the vertical axis represent the analytical values of the initial potential and kinetic energies ($U_o = u(0) * N_p / 2 = -2626.8$ hartrees, $K_o = k(0) * N_p = 74813$ hartrees, with $u(0)$ and $k(0)$ given by Eqs. (9) and (11) respectively) from which we can obtain an analytical value for the total system energy $E = 72186.2$. In the second panel, **Fig. 2(b)**, we have zoomed in on the first panel to observe the behavior of the system energy at the beginning of the simulation (note that the time axis goes from 0.0 to 5.0). We also moved $U(t)$ upward by 72000 hartrees to better appreciate the behavior of the kinetic and potential energies as the system moves towards equilibrium. Firstly notice that the (total) kinetic and potential energies correctly keep "sync" with each other to approximately conserve the (numeric) total energy $E_n(t) = K(t) - U(t) \sim const..$ The straight line is E and the (not so) straight line just below it is $E_n(t)$. Second, note how the potential energy moves upwards as time increases. Again this is due to the fact that at $t = 0.0$ we have an FCC lattice, which has a lower potential energy than a random configuration. Consequently, the potential energy tends to increase asymptotically towards an equilibrium value and the kinetic energy tends to *decrease* asymptotically to its own equilibrium value (corresponding to the system temperature). In the third panel **Fig. 2(c)**, we see the proton and electron "components" of the kinetic and potential energies. Note that the potential energies of electrons and protons are very close to each other (indeed, they are almost indistinguishable at this scale), but the kinetic components are quite separated. The electron kinetic energies are higher than the proton kinetic energies, or in other words, the electrons are at a higher

temperature than the protons; however, note also that we started *all particles with the same kinetic energy*. In Fig. 2(d) we plot the percent error in energy, which we define as

$$\%error = 100 \times \frac{E_n(t) - E}{E} \quad (16)$$

It can be seen that the $|\%error| < 1\%$ during the simulation. In fact, the worst error was $\sim 0.9\%$ at $t = 93.2$ and the mean of the absolute value was $\langle |\%error| \rangle \sim 0.22\%$. Also worth mentioning is that we have checked the numerical value of Γ and we obtained $\langle \Gamma \rangle = 0.0521$, in good agreement with the discussion given previously (see the discussion regarding Eq. (6)).

In Fig. (3) we see the behavior of the system momentum $P(t)$ as a function of time. Since there are no external forces acting on the system, the system momentum should be conserved. In Fig. 3(a) we plot the total system momentum as a function of time. We plot here the x , y and z components of the total momentum (p_x , p_y , p_z) as well as the magnitude of the total system momentum p_{tot} where

$$p_{tot} = (p_x^2 + p_y^2 + p_z^2)^{1/2} \quad (17)$$

Note that conservation of momentum holds quite well: not only is the total momentum well conserved but so are each of the three components. In Fig. 3(b) we see a plot of the “electron” component of the momentum and finally on Fig. 3(c) we see a plot of the “proton” component of the momentum. It can be seen that *most of the momentum is carried by the protons* (due to their higher mass).

In Fig. 4 we see four panels showing data for a specific particle, in this case an electron. In the first panel (Fig. 4(a)) we see a plot of the electron’s position as a function of time in the form of $x(t)$, $y(t)$, $z(t)$. At $t \sim 0.45$ $z(t)$ undergoes a large deflection, then $y(t)$ undergoes a large deflection at $t \sim 0.75$ and finally $x(t)$ also undergoes a large deflection at $t \sim 1.2$. Because we are using periodic boundary conditions the following constraint holds: $|x(t)| \leq L/2 = 1.664$ where L is the length of a side of the CB; the same relationship holds for $y(t)$, $z(t)$. In Fig.4 (b) we see a plot of the velocity as a function of time in the form of

$v_x(t), v_y(t), v_z(t)$. It can be seen that at $t=0.0$, the z-component was the largest component. In the following panel **Fig. 4(c)** we plot the cosine of the angle θ between this electron's initial velocity vector $v_o = v(t = 0.0)$ and its velocity vector as it evolves as a function of time $v = v(t)$, i.e., the relationship between these two vectors and θ is just $v_o \bullet v = \cos(\theta)$. We are interested in measuring the deflection time, defined as the time "in which deflections deflect the test particles by 90° " (Spitzer [3], p.131); by definition this is the time when $\cos(\theta) = 0.0$. In this case we found $t_D = 0.80$. Finally, we define the *Mean Free Path* λ as the distance the particle travels during the deflection time: in **Fig. 4(d)** we plot the particle's speed $v(t) = [v_x^2(t) + v_y^2(t) + v_z^2(t)]^{1/2}$ as a function of time. The integral of $v(t)$ from 0.0 to t_D gives us the electron's mean free path; here $\lambda = 7.6$ (the dashed vertical line denotes t_D). Note also that the electron's speed decreases slightly in accordance with the previous discussion regarding the kinetic energy (see Fig. 2(b)). It should also be noted that this electron deflection time was found not at equilibrium conditions but at $t = 0.0$. If we repeat the measurements (for the same electron) during the post-relaxation run ($t > 330.0$) we obtain $t_D = 1.0$ and $\lambda = 6.8$, so the values are quite similar to what we had at $t = 0.0$. In fact, we've found that in general there's no appreciable difference between deflection times found at $t = 0.0$ and at $t > 330.0$. The deflection time and the Mean Free Path of a proton were obtained in this case as well; these results are listed in Table VII.

It is interesting to compare these results with those given by Spitzer. If we use the formula for the deflection time assuming an ideal gas, we get an answer that is too large by about an order of magnitude. For a fully ionized gas we must use the equation (Spitzer [3], p. 132)

$$t_D = [8\pi n w p_o^2 (\Phi(x) - G(x)) \ln \Lambda]^{-1} \quad (18)$$

which gives the deflection time for a "test" particle. Here n is the "field" particles' number density (the field particles are all particles other than the "test" particle), w is the relative speed between the test particle and the field particles, $p_o = (\mu w)^{-1}$ (in this case; μ is the electron-proton reduced mass), $\Phi(x)$ is the error function and $G(x)$ is defined in Spitzer as

$$G(x) = (\Phi(x) - x\Phi'(x))/2x^2 \quad (19)$$

while x is defined to be

$$x = w\sqrt{\mu/2k_bT} \quad (20)$$

Spitzer lists values of $\Phi(x) - G(x)$ as a function of x . The quantity $\ln\Lambda$ is a way to take into account quantum-mechanical effects. Spitzer tabulates values of $\ln\Lambda$ as a function of temperature and density. However, for our problem the density is too high (approx. 9×10^{25} electrons/cm³) and so this theory breaks down and he does not list a value of $\ln\Lambda$ appropriate to our case. In spite of this, a crude extrapolation of his table allows us to estimate $\ln\Lambda \sim 1$; furthermore, our simulation is purely classical and no quantum effects were taken into account. We can take $w \sim (\langle v_e \rangle + \langle v_p \rangle)/2 \approx 5.8$ (see Table III below) and from this we get $x \sim 0.6$. Therefore, according to Spitzer, $\Phi(0.6) - G(0.6) \cong 0.42$ and so plugging into Eq. (18) we obtain $t_D \sim 1.3$. This is a bit larger than what we obtained, but it's still in good agreement.

In **Figure 5** we see a histogram of the instantaneous electron and proton speed distributions at the end of this first integration ($t = 330.0$). The values of the (instantaneous) mean speed and mean squared speed are also shown. The mean speed $\langle v \rangle$ was obtained first and the mean squared speed $\langle v^2 \rangle$ was obtained from

$$\langle v^2 \rangle = \langle v \rangle^2 + \sigma^2 \quad (21)$$

where σ^2 is the variance of the speed distribution. We represent relevant information about these distributions (plus the initial speeds at $t=0.0$) in the following table:

Table III: Speed characteristics at $t = 330.0$ plus initial speeds (all values in atomic units)

| Particle | Min. speed | $v(t=0.0)$ | $\langle v \rangle$ | $\sqrt{\langle v^2 \rangle}$ | Max. speed |
|--------------------|------------|------------|---------------------|------------------------------|------------|
| Electron | 1.63 | (12.2322) | 11.33 | 12.33 | 29.28 |
| Proton | 0.04 | (0.2854) | 0.26 | 0.28 | 0.70 |
| (el.)/(pr.) | 40.75 | (42.85) | 43.58 | 44.03 | 41.83 |

In the last row we divide the electron speed value by the proton speed value. In all cases the numbers are very close to the ratio of the square root of their masses $\sqrt{1836.2} = 42.85 \sim 43$. In the case of the initial speeds this ratio is exact by definition. Note that even the slowest electron is more than twice as fast as the fastest proton.

Finally in **Fig. 6** we plot the positions and velocities of all the particles at the end of this first integration. All positions have randomized by this time; note however, the apparent formation of a "chain" of particles towards the top of the CB. Again, the velocity vectors of most protons are too small to see at this scale, but those of electrons are clearly visible.

(b) Case $N_p = 1000$ particles (Post-Relaxation Run):

Once the system has relaxed, the program PLSMMD dumps the positions and velocities shown in **Fig. 6** as initial conditions used in the next program PLSMMD2. The reason we have written two separate programs is that once the system is relaxed we search for close approaches (an activity that is quite CPU intensive), especially between electrons and protons. To speed up the simulation we do not check for conservation of momentum (although we still check for energy conservation).

In **Fig. 7** we see four panels showing the four moments of the electron speed distribution, $\langle v \rangle$, $\langle v^2 \rangle$, $\langle v^3 \rangle$ and $\langle v^4 \rangle$ as a function of time ($0 \leq t \leq 440.0$). The straight horizontal lines represent the Maxwell-Boltzmann values and are given by

$$\langle v \rangle = 2 \left(\frac{2k_B T}{\pi m} \right)^{1/2} \quad (22a)$$

$$\langle v^2 \rangle = \frac{3k_B T}{m} \quad (22b)$$

$$\langle v^3 \rangle = 8 \left(\frac{2k_B^3 T^3}{\pi m^3} \right)^{1/2} \quad (22c)$$

$$\langle v^4 \rangle = \frac{15k_B^2 T^2}{m^2} \quad (22d)$$

where the q^{th} moment is given by

$$\langle v^y \rangle = \int_0^{\infty} v^y \bar{g}(v) dv \quad (23)$$

and \bar{g} is the MB speed distribution (Eq. (1) divided by the number density n , i.e., $\bar{g} = g/n$). $T = 1.56 \times 10^7$ K is the *equilibrium* temperature and k_B is Boltzmann's constant. It can be seen that at $t = 0.0$ the moments are far from the MB values and far from relaxation. However, as time increases, the moments tend to settle to some "quasi-relaxed" values slightly above the MB values. This gives us an estimate of the "relaxation time" for the electrons. We estimate a relaxation time for electrons $t_{re} \sim 84$ (2×10^{-15} s). We note that this value is quite a bit higher than that found at other N_p 's and this is due to the unusual upward "arching" of the moments at the beginning of the integration (especially noticeable in the second moment). The vertical dashed line at $t = 330.0$ separates the "relaxation" run from the "post-relaxation" run, while the values in the plots give the mean moments found for the range $330.0 < t \leq 440.0$ (past the relaxation time). The following table compares the empirically found values with the MB values given by Eqs. (22):

Table IV: Electron speed distribution moments

| Moment | Value | MB (Eqs. 22) | % Diff. |
|-----------------------|-------|--------------|---------|
| $\langle v \rangle$ | 11.35 | 11.22 | +1.1% |
| $\langle v^2 \rangle$ | 151.3 | 148.2 | +2.1% |
| $\langle v^3 \rangle$ | 2272 | 2217 | -2.5% |
| $\langle v^4 \rangle$ | 37542 | 36610 | +2.5% |

Note that the values are *higher* by 2% on average than what MB statistics predict. The electron speed distribution seems to have reached a "quasi-equilibrium" temperature that is higher than the temperature this problem would suggest. This "electron temperature" can be easily obtained from Eq. 22(b), this implies a temperature 2.1% higher than 1.56×10^7 K or approximately 1.60×10^7 K.

In **Fig. 8** we see four panels showing the moments of the speed distribution of protons. Again, as time increases the moments tend to relax to a "quasi-equilibrium" value, although the

time taken is longer than for electrons. It's hard to estimate the equilibrium time from the second moment but from third and fourth moment one could estimate $t_{\pi} \sim 280 (7 \times 10^{-15} \text{ s})$ for protons. Just as for electrons, we take the largest value to be the best approximation to the relaxation time, i.e., from the first moment one could estimate $t_{\pi} \sim 190$, but the third and fourth moments have clearly not yet relaxed. Note that in this case all four moments are lower than the MB values (at least after "relaxation"). In Table V we compare the empirical values found (again, for the range $330.0 < t \leq 440.0$) with the MB values obtained from Eqs. (22): recall that the mass of the proton is 1836.2 au:

Table V: Proton speed distribution moments

| Moment | Value | MB (Eqs. 22) | % Diff. |
|-----------------------|--------|--------------|---------|
| $\langle v \rangle$ | 0.2594 | 0.2618 | -0.9% |
| $\langle v^2 \rangle$ | 0.0792 | 0.0807 | -1.9% |
| $\langle v^3 \rangle$ | 0.0273 | 0.0282 | -3.2% |
| $\langle v^4 \rangle$ | 0.0104 | 0.0109 | -4.6% |

Here the empirically found moments are 2.7% *lower* on average than the MB values. The proton temperature implied by $\langle v^2 \rangle$ in this case is $1.54 \times 10^7 \text{ K}$. This is interesting because the average of the electron temperature and the proton temperature is very close to the Sun's core temperature. It seems that the higher the moment, the further away it is from MB; why this should be so is a puzzle.

What conclusion can we draw from these plots of the speed distribution? The distributions we have found seem consistent with what Lyman Spitzer wrote in his Physics of Fully Ionized Gases, so we will quote him directly (p. 136):

"We are now in a position to discuss what happens in a proton-electron gas, for example, when the velocity distribution is originally arbitrary. We assume that the mean kinetic energies of electrons and protons are of the same order of magnitude. Collisions of electrons with protons will deflect electrons and lead to an isotropic velocity distribution, but will not change appreciably the distribution of electron kinetic energies. Electron-electron collisions will gradually establish a Maxwellian velocity

distribution for the electrons, while proton-proton collisions will yield a corresponding velocity distribution for the protons, but at a kinetic temperature that may differ from the electron temperature. Finally, equipartition between electrons and protons is established by electron-proton collisions.”

What we have done is to integrate this “Coulomb” gas forward in time long enough for the distribution of both electrons and protons to have relaxed to “quasi-MB” values, but not so long that they have had time to come to thermal equilibrium with each other. Perhaps the electrons are “hotter” than protons due to their lighter mass. In any case, according to Spitzer, if we had integrated long enough past the “equipartition time” t_{eq} , electrons and protons should both have reached the same temperature. The equipartition time is approximately 43 times the collision time t_c for protons and 1836 times the collision time for electrons, where the collision time in seconds is given by (Spitzer [3], p. 133):

$$t_c = \frac{11.4\sqrt{AT^3}}{nZ^4 \ln \Lambda} \quad (24)$$

where A is the particle’s mass in terms of the *proton* mass, n is the number density of a given species (per cm^3), Z is the charge number ($Z = 1$ for both protons and electrons) and from our previous discussion, $\ln \Lambda = 1$. If we plug in numbers we obtain a collision time for electrons $t_{ce} \sim 2 \times 10^{-15}$ s and $t_{cp} \sim 8.6 \times 10^{-14}$ s for protons. Note that the collision time for electrons is identical to the relaxation time found previously, while for protons the agreement is off by an order of magnitude. Furthermore, note that according to Eq. (24), $t_{cp}/t_{ce} \cong 43$. If we estimate the equipartition time to be 1836 times the electron collision time then we obtain $t_{eq} \sim 1836 \times 80 = 154224$ (in au). With a time step size of 1.1×10^{-4} this would take 1.37×10^9 time steps (!) to achieve, a practical impossibility.

Finally we are interested in the speed distributions of proton-electron close approaches. At a given time step, whenever an electron approached within an arbitrary “small” distance R_m of a proton we recorded the positions and velocities for the pair; we called this a close-approach event or simply an “event”. The positions and velocities of the pair were recorded as long as the proton-electron distance r_{ij} remained smaller than R_m . This was done only during

the “post-relaxation” run; that is, during $330.0 < t \leq 440.0$. We define two types of events: *capture* and *escape*. A “captured” electron has, at a given r_y , a speed such that it cannot escape the Coulomb attraction of the proton while an “escaped” electron has enough speed (at a given r_y) to escape the Coulomb attraction. The boundary between these two cases is obtained from

$$\frac{1}{2} \mu v_{cr}^2 - (r_y^2 + \varepsilon^2)^{-1} = 0 \quad (25)$$

where μ is the electron-proton reduced mass, v_{cr} is the “critical speed”, and ε is the softening radius; this is just the relative kinetic energy plus the potential energy (corresponding to the force function of Eq. (14)). Solving for v_{cr} we obtain

$$v_{cr}^2 = \frac{2}{\mu \sqrt{(r_y^2 + \varepsilon^2)}} \quad (26)$$

This discussion is of course completely analogous to the concept of parabolic orbits in celestial mechanics. At a given electron-proton distance r_y (with $r_y \leq R_m$) we compute the pair’s relative speed $v_y = |\mathbf{v}_i - \mathbf{v}_j|$; if $v_y \geq v_{cr}$ then this is an “*escape event*”; otherwise it is a “*bound event*”. We have found a few cases where an electron was bound in orbit around a proton for several time-steps. In such a case, the same electron-proton pair will give rise to several consecutive bound-events. Such bound pairs can not last indefinitely because eventually other particles’ electrical forces will disrupt the bond. In any case, we are mainly interested in escape events and the relative speed distribution of such events. In Figure 9 we have three panels with various speed histograms. We used $R_m = 5.477 \times 10^{-3}$, about 2% of the Wigner-Seitz radius. In Figure 9(a) we have a histogram of v_y^2 for all close proton-electron approaches; there were 6008 “events”. Of these, only 2146 were escape events: in Fig. 9(b) we show a histogram of v_y^2 for the escape events only. The minimum relative speed squared was $(v_{i,j}^2)_{\min} = 345.01$ which is v_{cr}^2 at $R_m = 5.477 \times 10^{-3}$ while the average relative speed squared $\langle v_y^2 \rangle = 567.05$ and the maximum relative speed squared was found to be $(v_y^2)_{\max}$

=1354.0. The histogram “looks” like a MB energy distribution with the zero shifted to the right by the amount 345.01. All of these values are higher than the $\langle v^2 \rangle$ value obtained in Table IV (151.3) because of the proximity of the particles. In other words, the histogram shown in Fig. 9(b) is proportional to the energy distribution of passing electrons as “seen” from a proton’s point of view. For a real Coulomb force and not the modified version we’ve used here, all these values would be even higher. Going back to the alternative nuclear reaction $e^-(^3\text{He}, ^3\text{H})v_e$, recall that we need an electron with at least $18.6 \text{ keV} = 683.5 \text{ hartrees}$ to make the reaction feasible. Using the MB value of $\langle v^2 \rangle$ from Table IV, the average electron energy is approximately $\mu \langle v^2 \rangle / 2 \sim (0.999)(148.2)/2 = 74.0 \text{ hartrees}$, too low by almost an order of magnitude. If we now use the average relative energies of close approaches, we get $\mu \langle v_{ij}^2 \rangle / 2 \sim (0.999)(567.05)/2 = 283.2 \text{ hartrees}$ and using the maximum speed we get $\mu (v_{ij}^2)_{\text{max}} / 2 \sim (0.999)(1354.0)/2 = 676.3$, very close to the threshold value. It is clear that if we do take into account inter-particle forces, the relative energies increase. Furthermore, had we used a ^3He nucleus instead of a proton in the simulation all these relative energies would be higher by a factor of $Z = 2$ due to the higher charge of the ^3He nucleus. The specific values listed here are dependent on the arbitrarily chosen value of $R_m = 5.477 \times 10^{-3}$. A more formal analysis would use a value of R_m as the distance in which the electron and the ^3He nucleus “fuse” to become a Tritium nucleus (using the theory of nuclear beta decay).

If we think of the critical speed as the escape speed of electrons, then we can say that electrons with $v_{ij} = v_{cr}$ are on “quasi-parabolic” orbits. Electrons with $v_{ij} < v_{cr}$ are on “quasi-elliptical” bound orbits (pure, two-body orbits in this case are in general not closed due to the form of the force function, i.e., Eq. (14)). Meanwhile, electrons with $v_{ij} > v_{cr}$ are on “quasi-hyperbolic” orbits. A particle on a hyperbolic-like orbit would, in the limit of $r_{ij} \rightarrow \infty$, have a certain “excess speed” above zero (if it were zero we would have a parabolic-like orbit). For every event shown in Fig. 9(b) we have subtracted an amount corresponding to a parabolic orbit (given by Eq. (26)) and show the results in the last histogram, **Fig. 9(c)**: this is a histogram of the “excess speed squared”. The figure is a half-Gaussian with a standard deviation of $\sigma = 113$ and a mean value of $\langle v_{ij}^2 \rangle = 115.17$. It was expected that perhaps the values of $\langle v_{ij}^2 \rangle$ for the *excess speed* would be higher than the mean squared speed for an ideal

gas (i.e., $\langle v^2 \rangle = 148.2$), but this was not the case. We checked to see if this deficiency could be explained by Debye screening, but screening is a very small effect at this close range ($r_{ij} \leq R_m$) and does not account for the smallness of $\langle v_{ij}^2 \rangle$.

An attempt was also made to obtain histograms for electron-electron and proton-proton close approaches but these happened too infrequently to obtain useful data.

(c) Summary of Results:

In this section we summarize our results using $N_p = 512, 1000, 1728$ particles, which are presented in the form of tables. Again, the time step size is $\Delta t = 1.1 \times 10^{-4}$, and the outer "cut-off" radius $R_c = 0.67$.

In Table VI we show the electron deflection times plus the Mean Free Paths. The analytical mean free path is obtained from $\lambda = \langle v \rangle_{MB} t_D = (11.22)(1.3) = 14.6$. An asterisk means that we are taking the average value obtained starting from $t = 0.0$ and from $t = 330.0$, since, as we have seen for the $N_p = 1000$ case, the values do not vary much. The values are somewhat consistent with each other. It should also be noted that in all cases the Mean Free Paths are larger than the sides of the largest CB's side ($L_{max} = d(1728)^{1/3} \cong 4.0$).

Table VI: Electron Deflection Times & Mean Free Paths

| N_p | Deflection Time t_D | Mean Free Path λ |
|------------------|-----------------------|--------------------------|
| 512* | 1.9 | 26.6 |
| 1000* | 0.9 | 7.2 |
| 1728* | 1.1 | 9.6 |
| Spitzer (Eq. 18) | 1.3 | 14.6 |

In Table VII we show the deflection times plus the Mean Free Paths for protons. These values were measured only at $t = 0.0$. Unfortunately we could not obtain values for $N_p = 1728$. However, it is apparent that the measured deflection times are *higher* than Spitzer's

predictions. Theoretically we expect the Mean Free Paths of electrons and protons to be the same.

Table VII: Proton Deflection Times & Mean Free Paths

| N_p | Deflection Time t_D | Mean Free Path λ |
|------------------|-----------------------|--------------------------|
| 512 | 103.0 | 16.1 |
| 1000 | 206.0 | 52.1 |
| 1728 | na | na |
| Spitzer (Eq. 18) | 55.7 | 14.6 |

In Table VIII we show the values of the estimated relaxation times t_{rx} for protons and electrons. These relaxation times are a measure of how long it takes the speed distribution to relax from FCC lattice type initial positions and delta functions as the initial speed distributions. The means are also computed; as expected, the relaxation time for electrons is much shorter than that for protons due to the latter's higher mass and lower mean speeds.

Table VIII: Relaxation Times

| N_p | Electrons | Protons |
|-------|-----------|---------|
| 512 | 21 | 150 |
| 1000 | 84 | 280 |
| 1728 | 14 | 300 |
| Mean | 39.7 | 243.3 |

In Table IX we present the observed values of the first four moments of the electron speed distribution. Recall that these values were obtained only for the range $330.0 < t \leq 440.0$, i.e., the "post-relaxation" run ($330 < t \leq 424.28$ for the case $N_p = 1728$). Mean values were obtained and percent differences between these mean values and the MB values are also shown. It seems that the higher the number of particles, the higher the value of the moment. However, if we make the assumption that the higher the number of particles the more "accurate" the simulation is, the values seem to be converging "up" to some asymptote as the number of particles get higher. This is shown in **Figure 10** for the second moment: the

other moments show this type of behavior as well. It would be hard to justify a fit to find this convergent value with only three points, however

Table IX: Electron speed distribution moments ($330.0 < t \leq 440.0$)

| N_p | $\langle v \rangle$ | $\langle v^2 \rangle$ | $\langle v^3 \rangle$ | $\langle v^4 \rangle$ |
|--------------------|---------------------|-----------------------|-----------------------|-----------------------|
| 512 | 11.31 | 149.70 | 2231.00 | 36640.00 |
| 1000 | 11.35 | 151.30 | 2272.00 | 37540.00 |
| 1728* | 11.38 | 151.89 | 2283.40 | 37724.00 |
| Mean | 11.35 | 150.96 | 2262.13 | 37301.33 |
| MB | 11.22 | 148.20 | 2217.00 | 36610.00 |
| %Difference | 1.1% | 1.9% | 2.0% | 1.9% |

An asterisk means that the time range is $330 < t \leq 424.28$.

In Table X we show the values of the first four moments of the *proton* speed distribution for $330.0 < t \leq 440.0$ ($330 < t \leq 424.28$ for the case $N_p = 1728$). Again we take the average and compare it to the MB value. Here, the average values are lower, in contrast to the electron case. Interestingly, the higher the moment the further away the values are from MB. In **Figure 11** we show the values of the second moment as a function of the number of particles. Again, the empirical values seem to be converging “down” to some asymptotic value; the other moments seem to converge also.

Finally in Table XI we show the “mean relative speeds squared”, raw (that is, just what was directly measured $\langle v_{ij}^2 \rangle_{(raw)}$) and the “mean relative *excess* speed squared” $\langle v_{ij}^2 \rangle_{(excess)}$. The relationship between these two is

$$\langle v_{ij}^2 \rangle_{(excess)} = \langle v_{ij}^2 \rangle_{(raw)} - v_{cr}^2 \quad (27)$$

where v_{cr}^2 depends on the relative electron-proton distance r_{ij} and is given by Eq. (26). Note that the mean squared excess speed raw (113.66), is smaller than the mean squared speed assuming a MB distribution (148.20).

Table X: Proton speed distribution moments ($330.0 < t \leq 440.0$)

| N_p | $\langle v \rangle$ | $\langle v^2 \rangle$ | $\langle v^3 \rangle$ | $\langle v^4 \rangle$ |
|--------------|---------------------|-----------------------|-----------------------|-----------------------|
| 512 | 0.2600 | 0.0799 | 0.0277 | 0.0105 |
| 1000 | 0.2594 | 0.0792 | 0.0273 | 0.0104 |
| 1728* | 0.2601 | 0.0791 | 0.027 | 0.01 |
| Mean | 0.2598 | 0.0794 | 0.0273 | 0.0103 |
| MB | 0.2618 | 0.0807 | 0.0282 | 0.0109 |
| %Diff | -0.8% | -1.6% | -3.1% | -5.5% |

An asterisk means that the time range is $330 < t \leq 424.28$.

Table XI: Mean relative speeds squared. raw and excess

$$(R_m = 5.477 \times 10^{-3}, 330.0 < t \leq 440.0)$$

| N_p | $\langle v_{ij}^2 \rangle_{(raw)}$ | $\langle v_{ij}^2 \rangle_{(excess)}$ |
|--------------|------------------------------------|---------------------------------------|
| 512 | 570.50 | 113.50 |
| 1000 | 567.05 | 115.17 |
| 1728* | 566.44 | 112.31 |
| Mean | 568.0 | 113.66 |

An asterisk means that the time range is $330 < t \leq 424.28$.

V. CONCLUSIONS/SUMMARY

We have integrated a simplified model of a plasma forward in time using a Molecular Dynamics approach. The total number of particles was varied and results with different N_p were compared. This plasma is a fully ionized gas consisting of protons and free electrons and has the same temperature and density as is found in the core of the Sun. We wished to investigate whether inter-particle forces (the Coulomb force) in this multi-body problem might be a source of deviations from MB statistics predictions, which are strictly true for an ideal gas. Specifically we wished to see if the reaction given by Eq. (4), $e^{-}({}^3\text{He}, {}^3\text{H})\nu_e$, [$Q = -18.6$ keV] might be made more likely than standard solar theory predicts due to multi-body effects. The plasma was integrated from non-equilibrium initial conditions (FCC lattice for positions and a delta function for the speed distribution) until quasi-equilibrium was reached. During this time we checked the deflection times, the mean free paths and the relaxation times (from

the first four moments) for electrons and protons. The results were somewhat consistent with analytical results as provided by Spitzer [3], especially for electrons.

After the system was completely “quasi-relaxed”, we again propagated the system forward in time and collected statistics on the first four moments of the proton and electron speed distributions as well as statistics on close inter-particle approaches. The first four moments of the speed distribution were recorded for the duration of the post-relaxation run and the average results were compared to the MB values. A curious phenomenon is that, although we started protons and electrons with the same kinetic energies, electrons quickly gained kinetic energy at the expense of protons. Therefore, electrons were slightly “hotter” (+1.9%) and protons were slightly cooler (-1.6%) than the system temperature of 1.56×10^7 K (see Tables IX and X). However, this is not at all inconsistent with the behavior of a fully ionized gas, as shown by Spitzer [3]. Note that the average of the electron (1.59×10^7 K) and proton temperatures (1.53×10^7 K) is very close to the system temperature. To have the plasma in true equilibrium we would have to have integrated the system past the “equipartition time”, where protons and electrons would have the same temperature. As we have seen, this would be out of the question with the present approach. This is why we prefer to call the plasma “quasi-relaxed” and not relaxed at the end of the integration.

A way we used to measure deviation from MB was to look at the first four moments during “quasi-equilibrium” ($t > 330.0$) and compare the values with MB. The electron moments were higher (+1.7% on average) than MB and the proton moments were lower (-2.8% on average) than MB. However, it is likely that the observed deviations from MB are consistent with the plasma not being in complete thermal equilibrium.

What about close approaches between electrons and protons? We do have to use the total relative energy and not just the kinetic energies. For example in the $N_p = 1000$ particles case, we had that the mean relative kinetic energy was $\langle k \rangle = 283.2$ hartrees, but the mean relative potential energy in this case was $\langle u \rangle = -\left[\mu \sqrt{r_y^2 + \epsilon^2}\right]^{-1} = -226.4$ hartrees for a total mean relative energy of $\langle e \rangle = 56.8$ hartrees, lower than even the MB relative energy of 74.0 hartrees and quite low compared to the threshold energy for the reaction $e^-(^3\text{He}, ^3\text{H})\nu_e$, [$Q = -683.5$ hartrees]. Note that, relative to the MB case, the inter-particle forces seem to have

actually *decreased* the mean relative energies, possibly making the rate of the reaction $e^{-}({}^3\text{He}, {}^3\text{H})\nu_e$ less likely than in the pure MB case. As previously stated, the mean squared excess speed raw (113.66), is smaller than the MB mean squared speed (148.20).

We conclude that the observed deviations from a MB distribution are probably not significant enough to make the alternative reaction $e^{-}({}^3\text{He}, {}^3\text{H})\nu_e$ more likely than in a pure MB case. Indeed, the observed deviations are in accordance with the expected behavior of a plasma, as described by Spitzer. Deviations from MB due to electron degeneracy (protons are practically non-degenerate) were also explored analytically as an aside project. At the temperature and pressure found at the core of the Sun, the mean electron energy is about 3% higher in the degenerate case than in the MB case. Again, this is probably too small an effect to make a difference. It seems that, in light of recent investigations regarding neutrino “flavor changes”, a possibly better explanation for the deficiency of neutrinos from the Sun may be *neutrino oscillations*, or the MSW effect [17, 18]. Very briefly, neutrinos exist in three types: electron-neutrino (ν_e), which is the only type that is produced in the Sun, the muon-neutrino (ν_μ) and the tau-neutrino (ν_τ). Recent experiments at the Super-Kamiokande neutrino detector in Japan have suggested that oscillations indeed take place in the case of the tau and muon neutrinos and possibly in the case of electron-neutrinos [19]. This implies that neutrinos have mass, contrary to standard particle physics, which assumes zero mass for them. If oscillations do take place, as (electron) neutrinos from the Sun travel to Earth, they could switch to either of the other two types (tau and muon). With the exception of the Sudbury Neutrino Observatory in Canada, which can detect all three flavors and will test the MSW effect, present-day “neutrino telescopes” can only detect one or two types of neutrinos at a time. If neutrinos oscillate, the deficiency of solar neutrinos may be only an apparent one, as the detectors only detect neutrinos of one flavor (electron) or the other, thus possibly explaining the solar neutrino problem. Therefore, it may be that the answer to the solar neutrino problem may lie in particle physics, not statistical mechanics.

VI. FIGURES AND FIGURE CAPTIONS

FIGURE 1: Initial conditions (positions and velocities) for the particular case $N_p = 1000$ particles. Initial positions correspond to an FCC lattice. Only the velocity vectors of the electrons can be seen.

FIGURE 2: Behavior of the system energy for the case $N_p = 1000$. (a) System energy (kinetic, total and potential). (b) System energy but with the potential energy increased by 72000 hartrees. (c) System energy separated into proton and electron components. (d) Percent error in the total energy.

FIGURE 3: Behavior of the system momentum for the case $N_p = 1000$. (a) Total and x, y, z components of the system momentum. (b) Electron x, y, z momentum components. (c) Proton x, y, z momentum components.

FIGURE 4: Behavior of a given particle (in this case particle number 18, an electron) as a function of time for the case $N_p = 1000$. (a) Position as a function of time (shown in the form of components). (b) Velocity as a function of time (shown in the form of components). (c) Cosine of the angle between the initial velocity vector v_0 and the velocity vector as a function of time $v(t)$. Circle represents the deflection time (here 0.80). (d) Speed of the particle as a function of time, $v(t)$ vs. t . The dashed vertical line corresponds to the deflection time and the integral of $v(t)$ from zero to the deflection time gives the mean free path (here equal to 7.6 time units).

FIGURE 5: Speed histograms for electrons (panel a) and protons (panel b) for the case $N_p = 1000$ at the end of the “relaxation run” ($t = 330.0$).

FIGURE 6: Final conditions (positions and velocities) for the particular case $N_p = 1000$ particles at the end of the “relaxation run” ($t = 330.0$). Only the velocity vectors of the electrons can be seen.

FIGURE 7: First four moments of the electron distribution as a function of time for the case $N_p = 1000$. The horizontal lines represent the Maxwell-Boltzmann values.

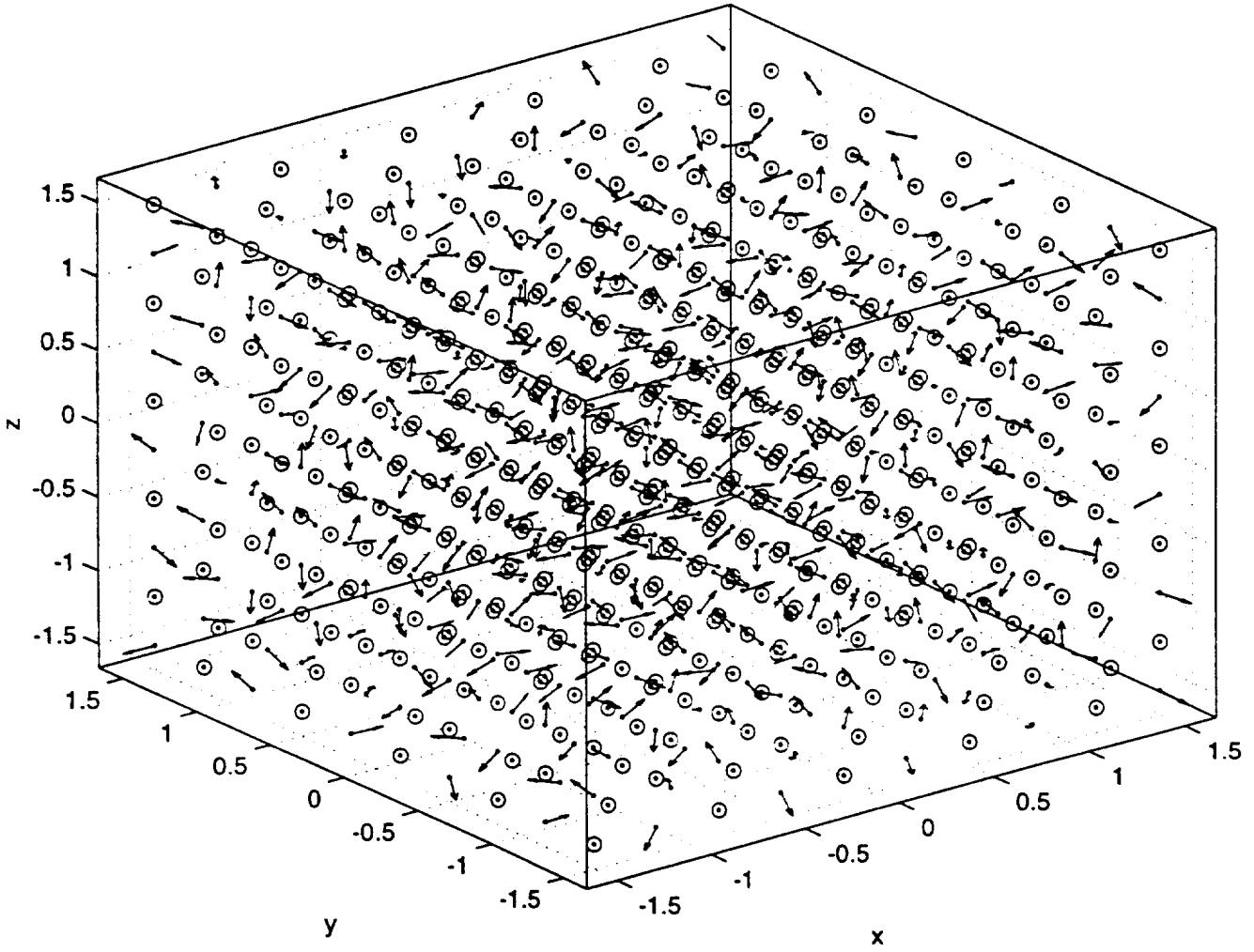
FIGURE 8: First four moments of the proton distribution as a function of time for the case $N_p = 1000$. The horizontal lines represent the Maxwell-Boltzmann values.

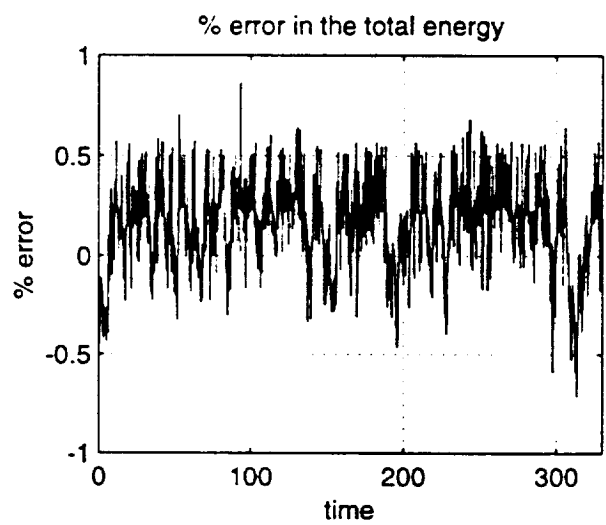
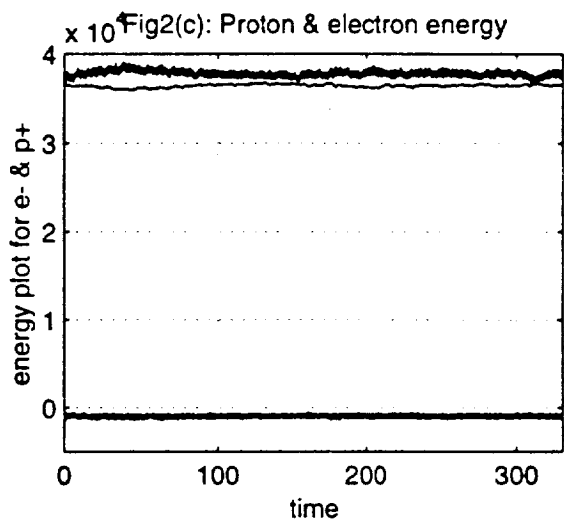
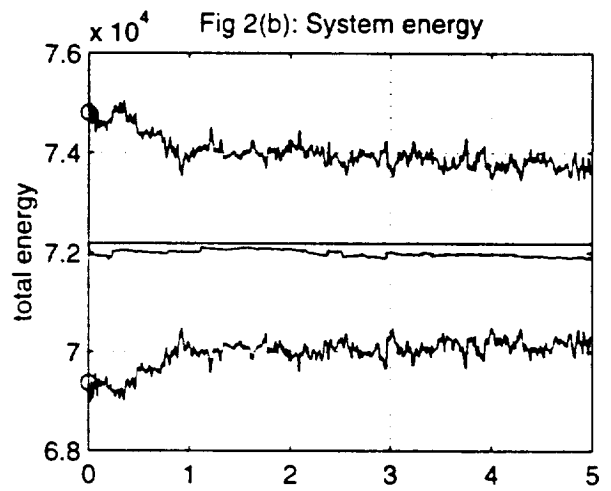
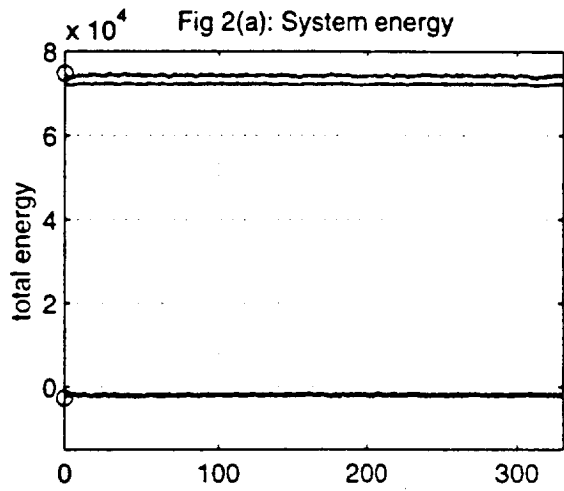
FIGURE 9: Distributions of squared speed for close electron-proton approaches $N_p = 1000$ and $R_{in} = 0.005477$. These "events" cover the period of the "post-relaxation" run $330.0 < t \leq 440.0$. (a) Histogram of the squared speed for all events. (b) Histogram of the squared speed for escape events only. (c) Histogram of the squared speed minus the critical speed. In other words, histogram of the excess speed squared.

FIGURE 10: Empirical values of the mean squared speed $\langle v^2 \rangle$ for electrons as a function of the number of particles (cases $N_p = 512, 1000, 1728$). It can be seen that the mean value is higher than the Maxwell-Boltzmann value.

FIGURE 11: Empirical values of the mean squared speed $\langle v^2 \rangle$ for protons as a function of the number of particles (cases $N_p = 512, 1000, 1728$). It can be seen that the mean value is lower than the Maxwell-Boltzmann value.

Fig. 1: Initial conditions ($t = 0.0$; $N_p = 1000$)





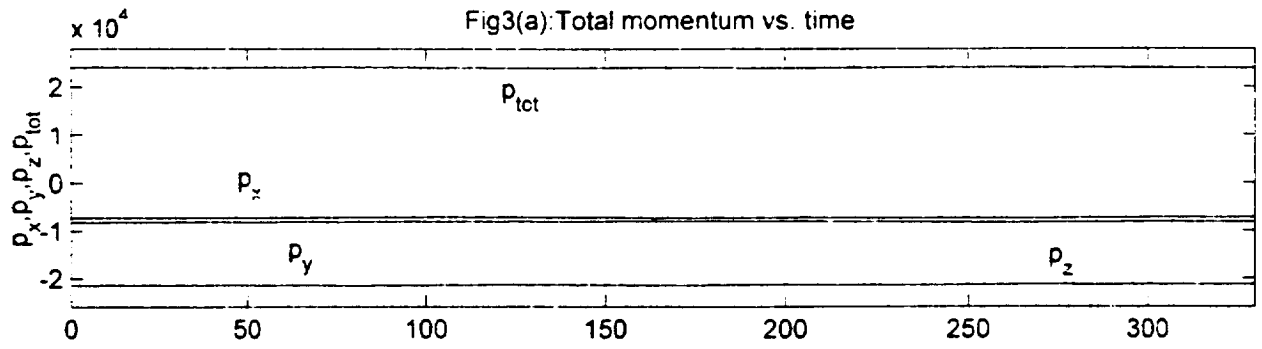


Fig 3(b): electron momenta

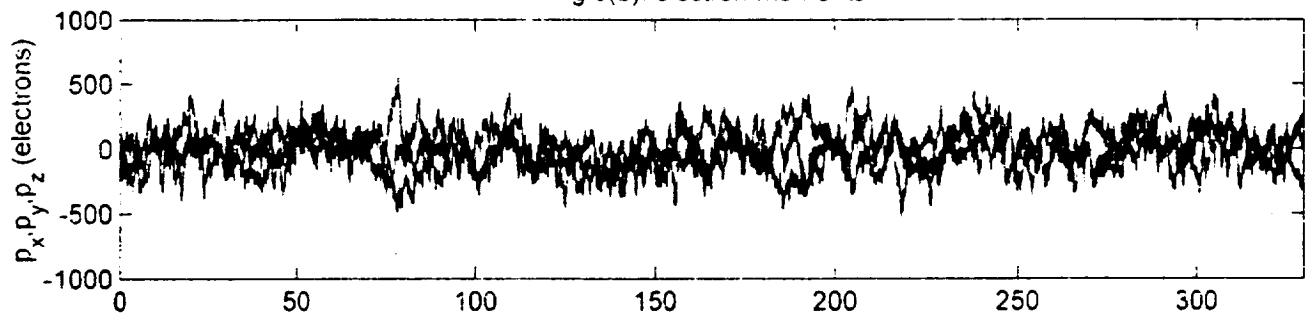
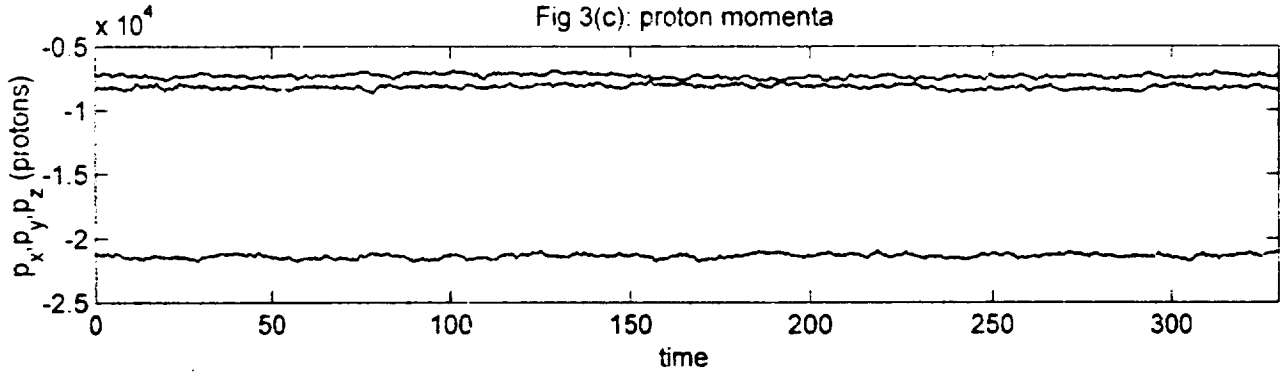


Fig 3(c): proton momenta



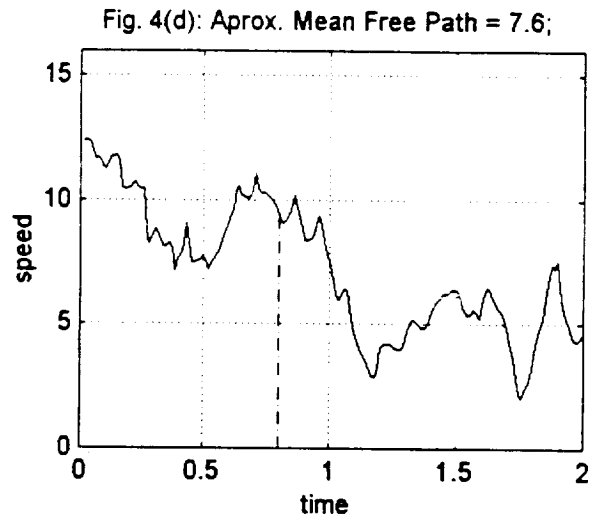
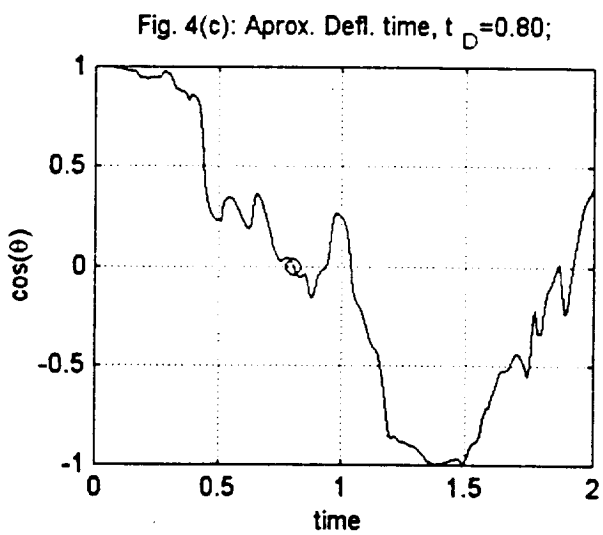
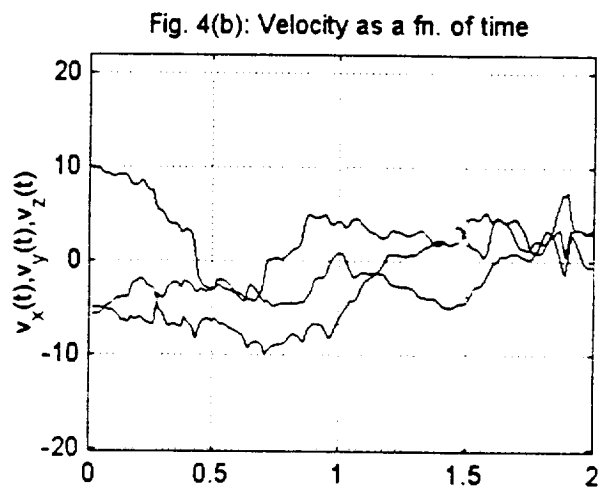
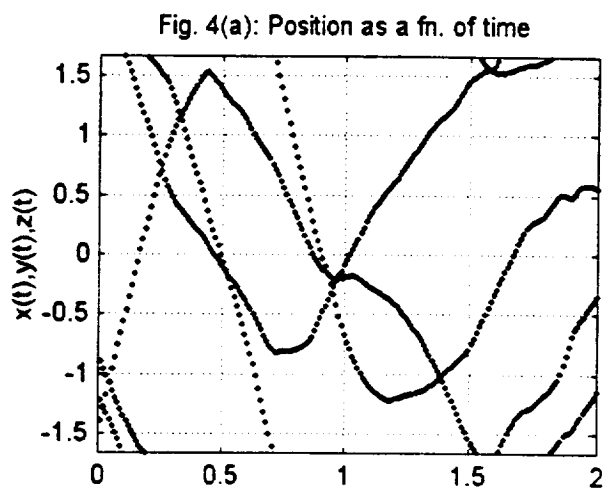


Fig. 5(a): $N_e=500$; Time=330

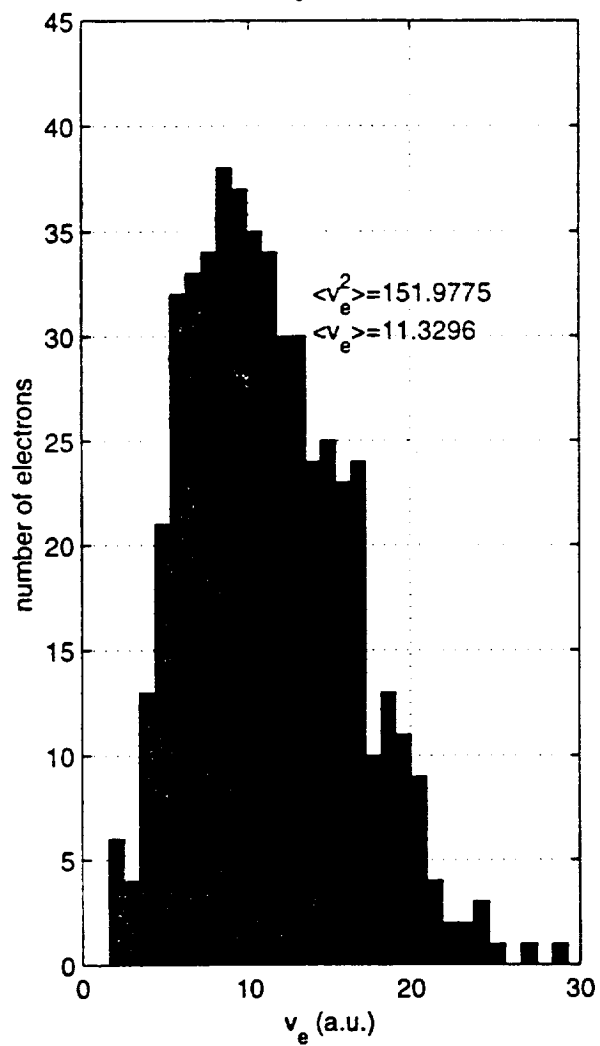


Fig. 5(b): $N_p=500$; Time=330

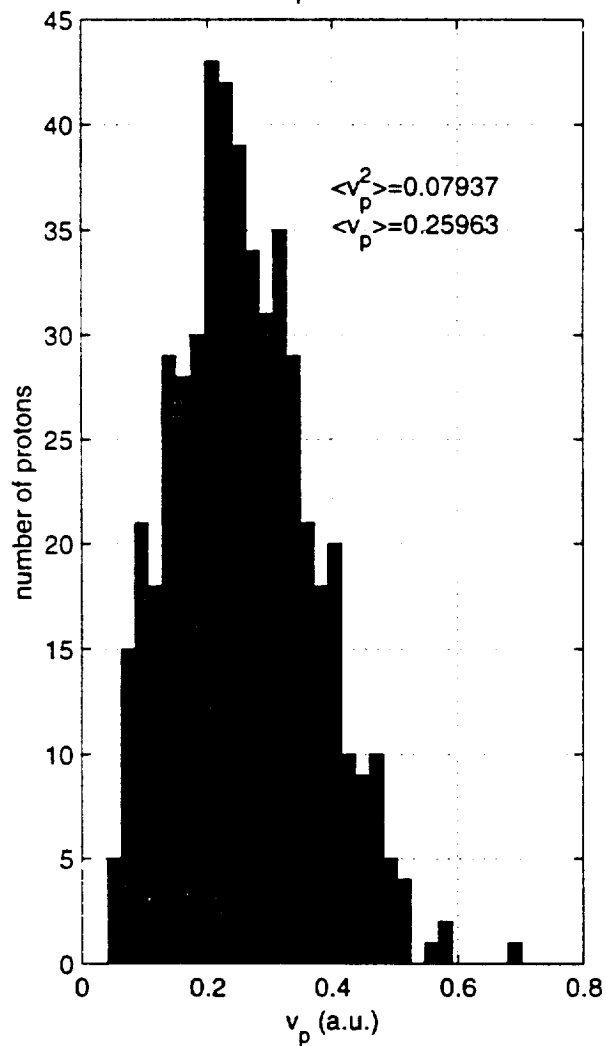


Fig. 6: Final conditions ($t = 330.0$; $N_p = 1000$)

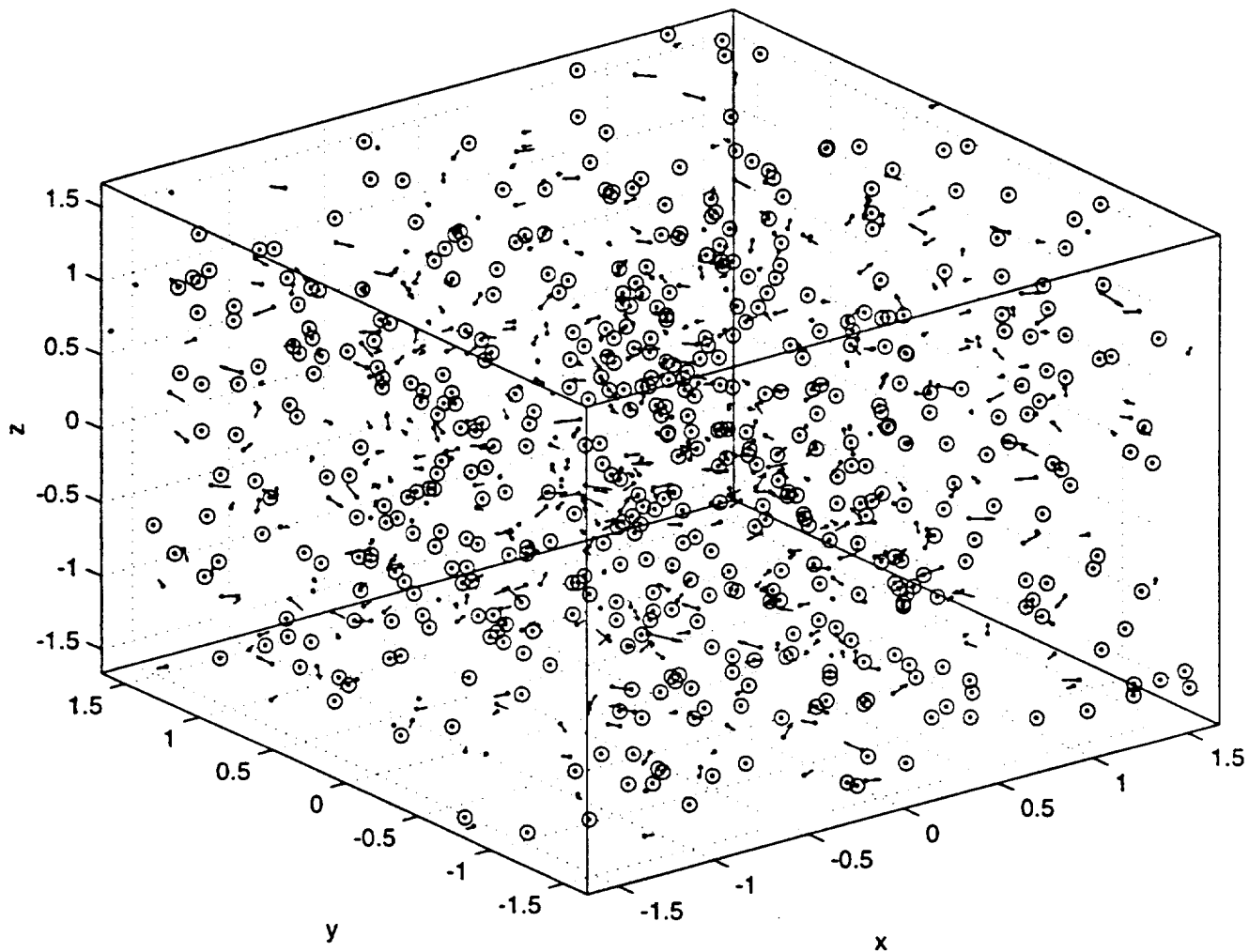


Fig. 7: First 4 moments of the e^- speed distribution ($N_e=500$)

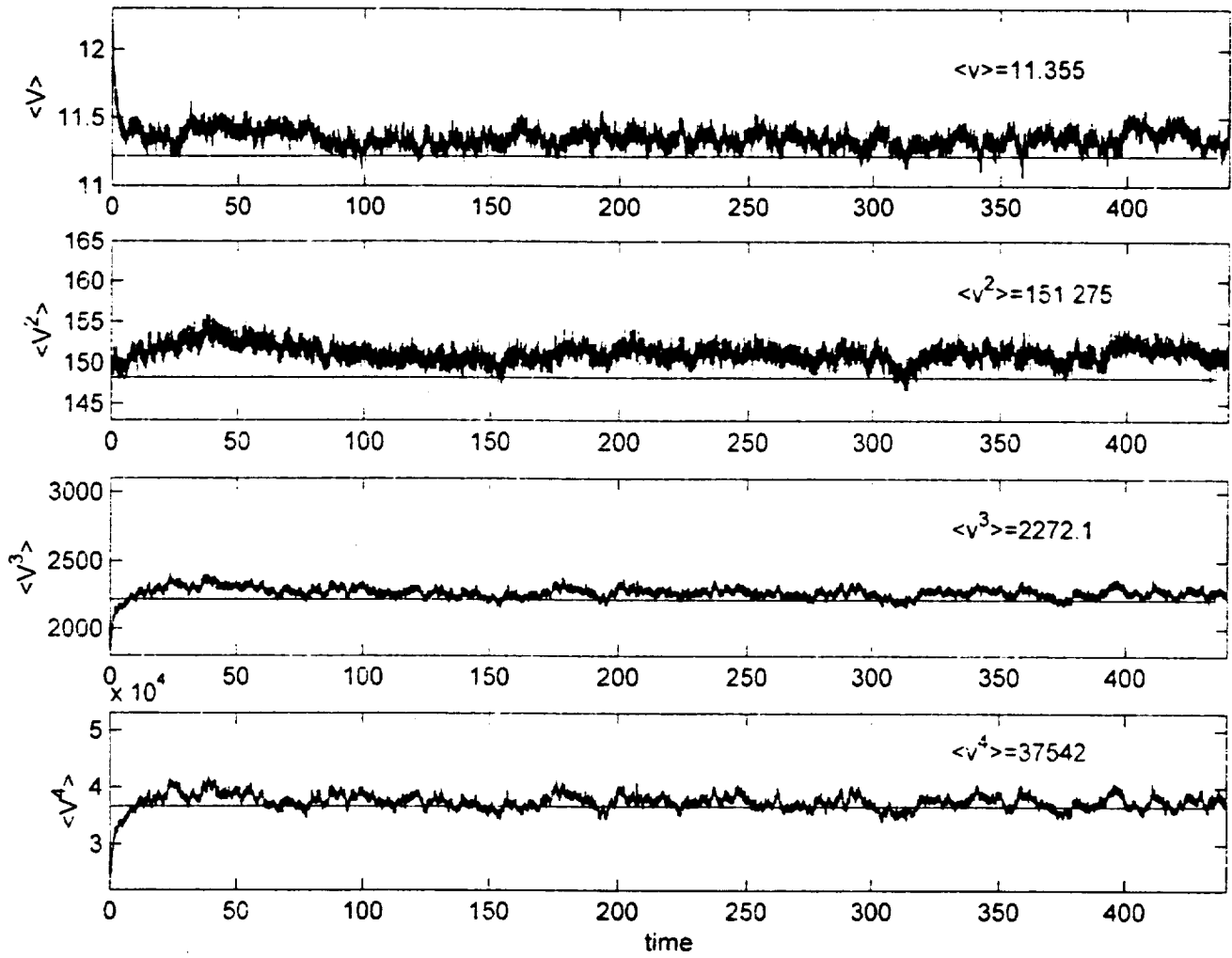


Fig. 8: First 4 moments of the p^+ speed distribution ($N_p=500$)

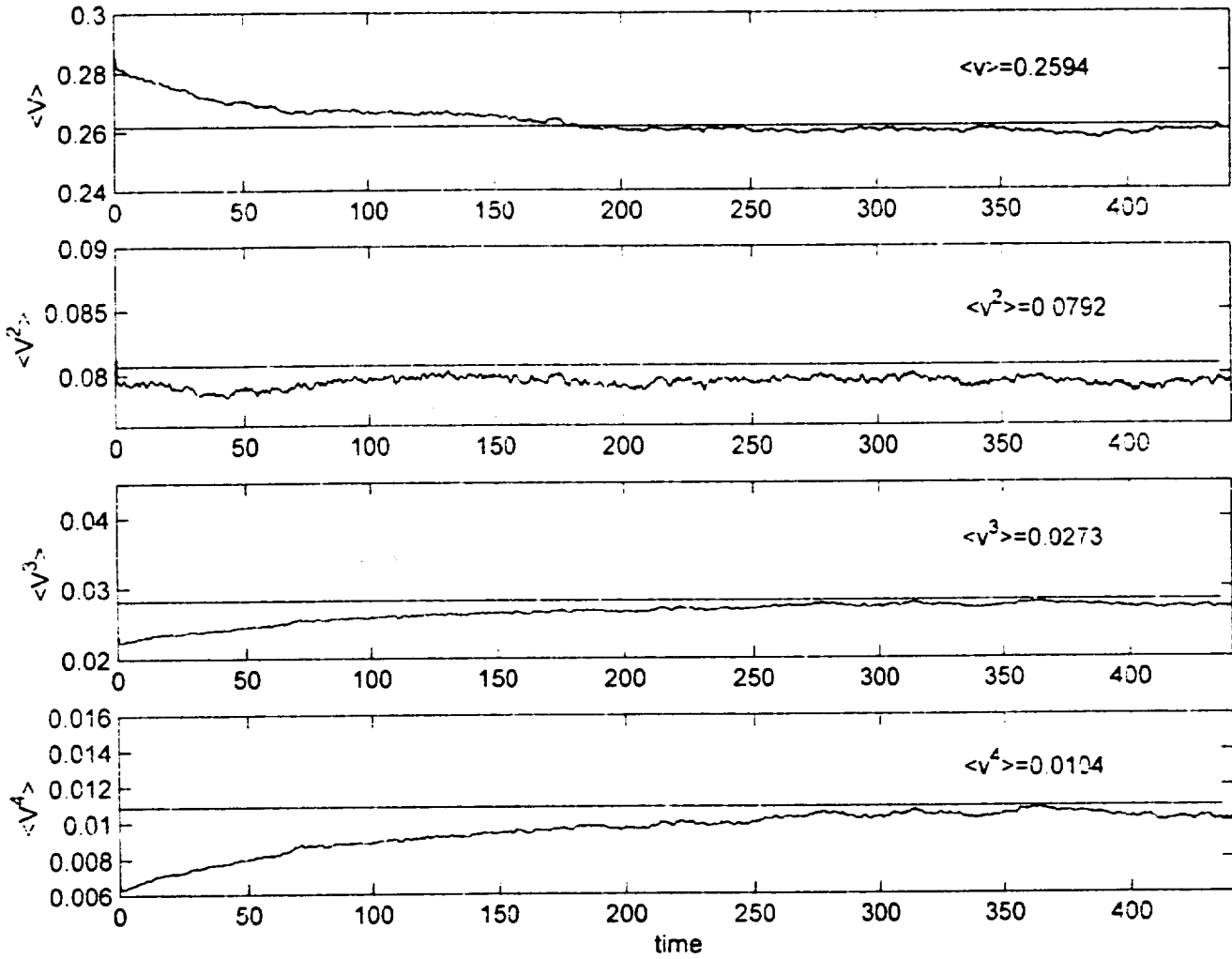


Fig. 9: (ELECTRON-PROTON); $R_{iA} = 0.005477$; $330.00 < t < 440.00$;

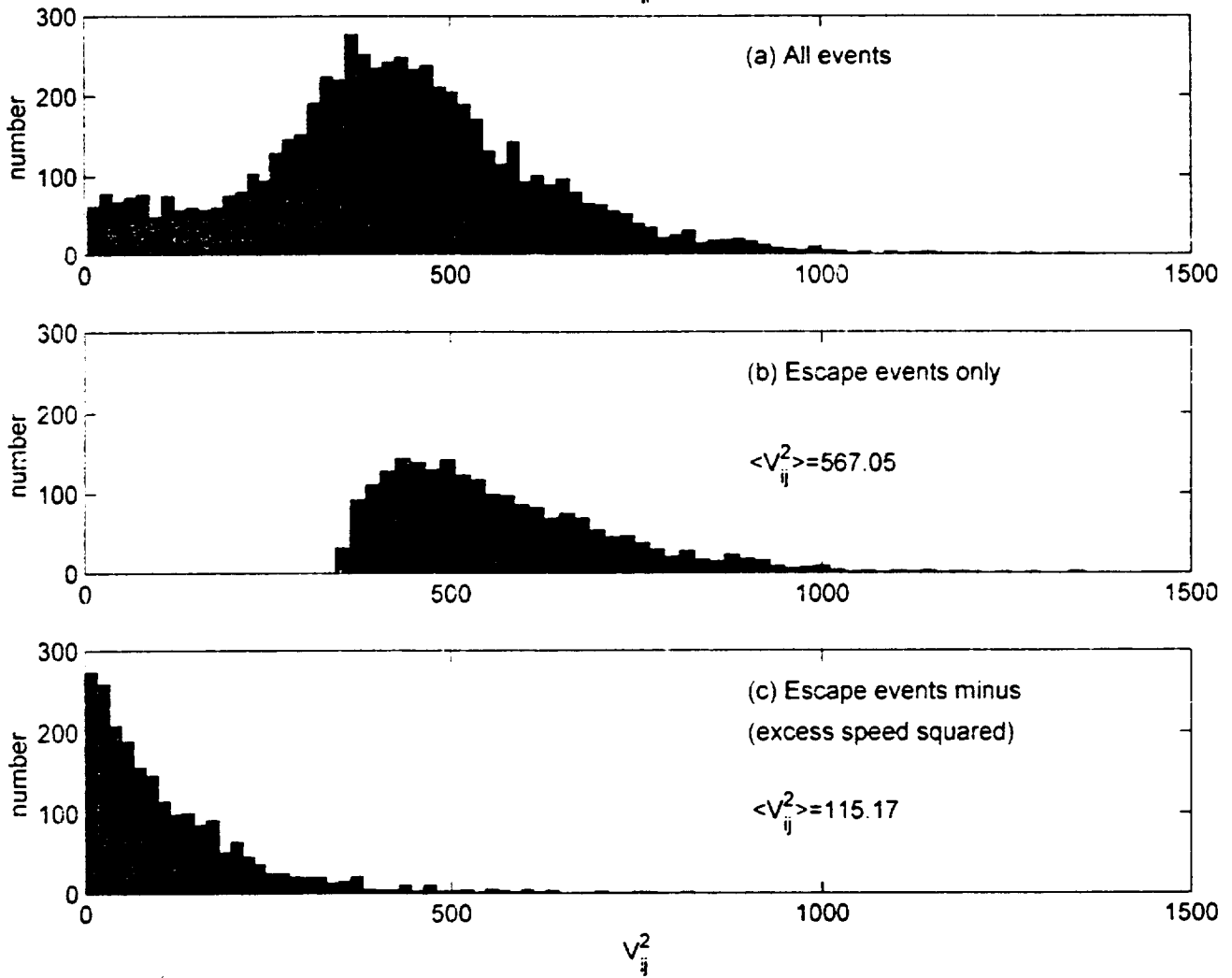


Figure 10: Second moments as a function of N_p

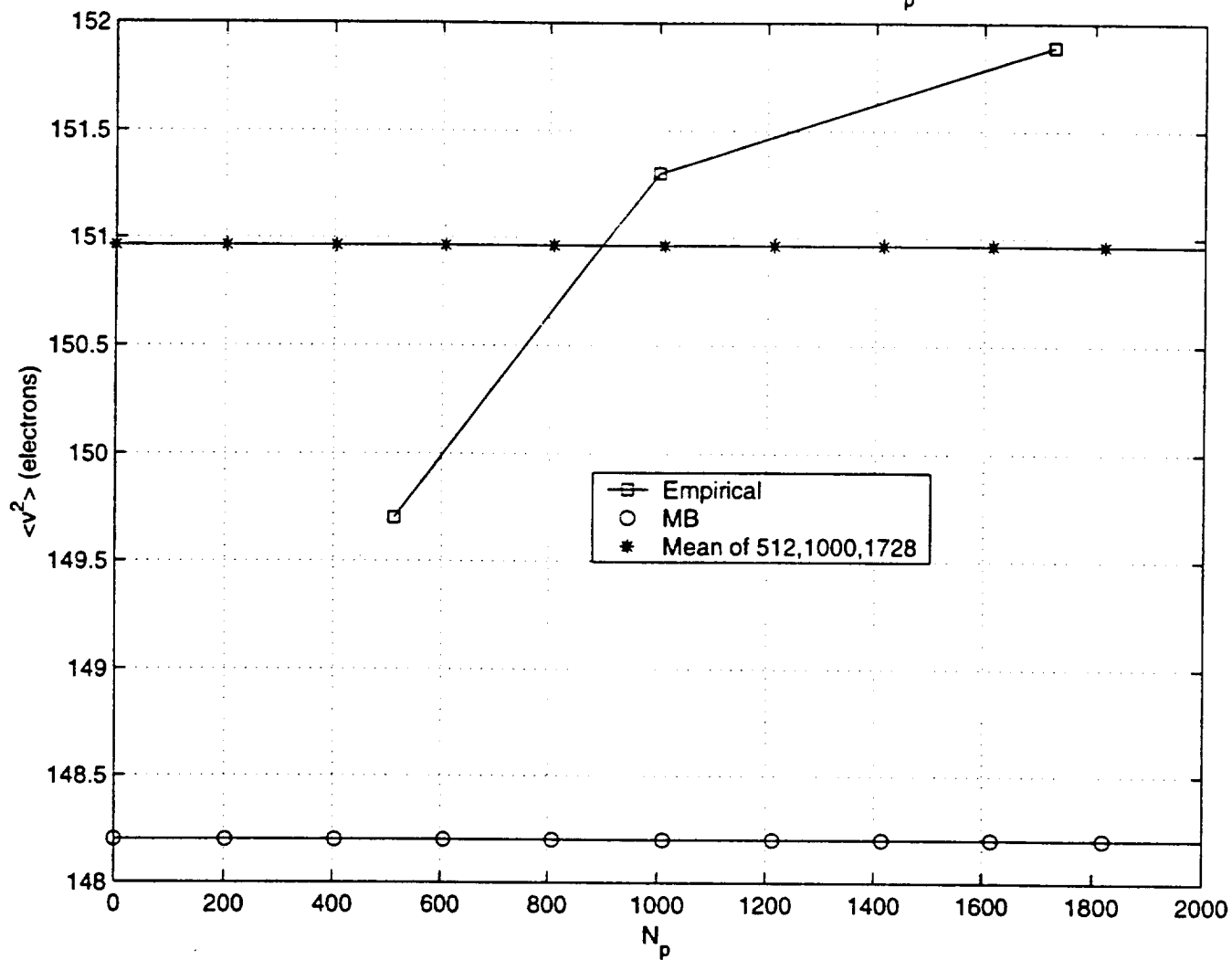
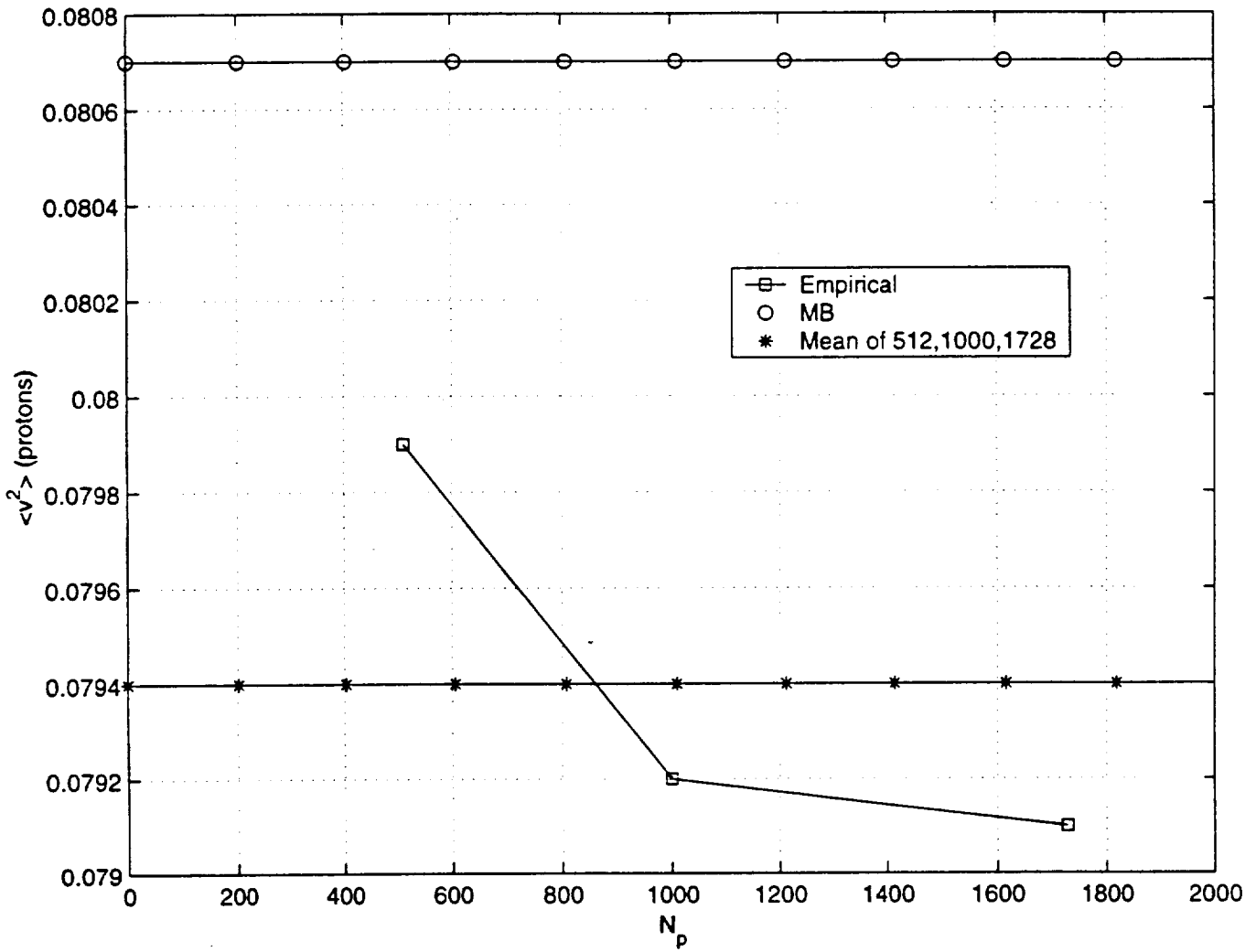


Figure 11: Second moments as a function of N_p



VII. REFERENCES

- [1] Bahcall, J.N, Calaprice, F; McDonald, A.B. and Totsuka, Y. 1996. Solar neutrino experiments: The next generation. *Physics Today*. 47(7):30-36.

- [2] Chen, F. 1984. *Introduction to Plasma Physics and Controlled Fusion. Volume 1: Plasma Physics*. New York, NY: Plenum Press.

- [3] Spitzer, L. 1965. *Physics of Fully Ionized Gases*. New York, NY: Interscience Publishers.

- [4] Swihart, T. L. 1972. *Physics of Stellar Interiors*. Pachart Publishing House, Tucson AZ.

- [5] Clayton, D. 1974. Maxwellian relative energies and solar neutrinos.. *Nature*. Vol. 249.

- [6] Clayton, D. 1975. Solar models of low neutrino-counting rate: the depleted maxwellian tail. *The Astrophysical Journal*, 199: 494-499.

- [7] Clayton, D. 1983. *Principles of Stellar Evolution and Nucleosynthesis*. The University of Chicago Press, Chicago.

- [8] Bahcall, J.N. 1989. *Neutrino Astrophysics*. Cambridge University Press, New York NY.

- [9] Bahcall, J.N., Wolf, R. 1963. Terminating the proton-proton chain at high densities. *Atrophysical Journal*, 139:622.

- [10] Haile, J. M. 1992. *Molecular Dynamics Simulations*. New York, NY: Wiley Interscience.

- [11] McQuarrie, D. M. 1983. *Quantum Chemistry*. Mill Valley, CA. University Science Books.

- [12] Ashcroft, N. W., Mermin, N. D. 1976. *Solid State Physics*. Fort Worth, TX. Saunders College Publishing.

[13] Allen, M.P., Tildesley, D.J. 1989 *Computer Simulation of Liquids*. Oxford University Press.

[14] Swope, Andersen, Berens and Wilson. 1982 Physical clusters of molecules. *Journal of Chemical Physics*. 76.

[15] Sellwood, J. A. 1987. The Art of N-Body Building. In *Annu. Rev. Astron. Astrophys.* Vol. 25. 1987 25: 151-186.

[16] Hockney R.W. Eastwood, J.W. 1988. *Computer Simulations Using Particles*. Adam Hilger.

[17] L. Wolfenstein, Phys. Rev. **D17**, 2369 (1978); **D20**, 2634 (1979);.

[18] S. P. Mikheyev and A. Yu. Smirnov, Yad. Fiz. **42**, 1441 (1986); [Sov. J. Nucl. Phys. **42**, 913 (1986)]; Nuovo Cimento **9C**, 17.

[19] Kearns, E. Kajita, T., Totsuka, Y. (1999). Detecting Massive Neutrinos. *Scientific American*. August Issue. 64-71.

Relevant Web Sites:

[a] John Bahcall's home page: <http://www.sns.ias.edu/~jnb/>. John Bahcall is one of the world's leading researchers on the solar neutrino problem.. Contains the abstracts of many of his papers related to neutrino physics. Also contains many useful links regarding the solar neutrino problem.

[b] Canada's Sudbury Neutrino Observatory (SNO) home page: <http://www.sno.phy.queensu.ca>

[c] Super-Kamiokande Web site at Boston University: <http://hep.bu.edu/~superk/index.html>

[d] Juha Peltoniemi's Ultimate Neutrino Page at <http://www.physics.helsinki.fi/neutrino>

VIII. ACKNOWLEDGMENTS:

Jose Luis Alvarellos would like to thank Peter Cheeseman for suggesting this problem for research. I have learned much about the Solar Neutrino Problem and its importance in the overall scheme of unsolved (soon to be solved?) astrophysical problems. I would also like to thank Patrick Hamill and Alejandro Garcia, both of the SJSU Physics Department, the former for all the help and encouragement and the latter for all the interesting conversations regarding statistical mechanics. Also would like to thank my wife Alejandra and my son Jose Luis Jr. for all their patience and encouragement throughout this project. Last but not least, I want to thank the San Jose State University Foundation for all their support. This research was supported by NASA's grant number NCC 2-5248.

APPENDIX:

Inputs to and programs PLSMMD.FOR & PLSMMD2.FOR

The first thing to decide before running these two programs is the number of particles. Recall that the number of particles is restricted by the condition $N_p = 8i^3$ where $i = 1, 2, 3, 4, 5, 6, \dots$ etc. or $N_p = 8, 64, 216, 512, 1000, 1728$. In this "experiment" we only considered $512 \leq N_p \leq 1728$. Once the number of particles has been decided upon, the FORTRAN include file **PLASMA.INC** is edited with a text editor and the number of particles is entered, where it is defined a PARAMETER:

```
C ....THE TOTAL NUMBER OF PARTICLES
C.....NP=64,216,512,1000,1728,..., 8*I^3 (I=1,2,3...)
      INTEGER NP
      PARAMETER(NP = 512)
```

The program **PLSMMD.FOR** is then compiled. Now we have the executable, which needs an input file stating the number of time-steps, the time-step size, etc. The contents of this input file **IN.DAT** are as follows:

| | |
|---------|---|
| 0.26 | The Wigner-Seitz radius, in atomic units (au) |
| 1.56e7 | The temperature, in Kelvin |
| 1000000 | The number of time steps |
| 1.1e-4 | The time-step size (au) |
| 0.67 | "Outer" cut-off radius (au) |
| 18 | Particle number to follow (output in file TXYZ.DAT) |
| 100 | How often to write energies file ENERGY.DAT (# of time-steps) |

| | |
|-----|--|
| 15 | How often to update the neighbor lists (# of time-steps) |
| 0.5 | Max. % error allowed in energy |

Once the program **PLSMMD.FOR** is finished, it outputs the file **IN2.DAT**, which is the input file for the program **PLSMMD2.FOR**. The contents of the file **IN2.DAT** are as follows:

| | |
|-------------------|--|
| 512 | Total # of particles (used as a check) |
| 330.0 | Time at the end of the first run [computed by PLSMMD.FOR] |
| 0.26 | Wigner-Seitz radius, in atomic units (au) |
| 15600000.000000 | Temperature, in Kelvin |
| 1000000 | Total # of time-steps |
| 1.10D-04 | Time-step size (au) |
| 0.67 | "Outer" cut-off radius (au) |
| 18 | Particle number to follow (output in file TXYZ2.DAT) |
| 100 | How often to write energies file ENERGY2.DAT (# of time-steps) |
| 15 | How often to update the neighbor lists (# of time-steps) |
| 1 | How often to check close approaches (# of time-steps) |
| 0.00547722557052 | How close particles can approach to record relative pos., vel. |
| 36959.274946828 | Total energy (hartree) [computed by PLSMMD.FOR] |
| -290.94705096300 | Corr. to the potential energy (hartree) [computed by PLSMMD.FOR] |
| 0.500000000000000 | Max. % error allowed in energy |

The first number is used as an internal check to make sure the two programs are compiled to the same number of particles. Note that some of the numbers are computed by the program **PLSMMD.FOR** and the user is not allowed to change them (for example, the time at the end of the **PLSMMD.FOR** run), lest there be inconsistencies in the two programs.